



# 1 **Oblique rifting triggered by slab tearing and back-arc extension : the** 2 **case of the Alboran rift in the eastern Betics**

3  
4 Marine Larrey<sup>1,2</sup>, Frédéric Mouthereau<sup>1\*</sup>, Damien Do Couto<sup>3</sup>, Emmanuel Masini<sup>4</sup>, Anthony  
5 Jourdon<sup>5</sup>, Sylvain Calassou<sup>2</sup> and Véronique Mieggebielle<sup>2</sup>

6 <sup>1</sup>Université Paul Sabatier, Géosciences Environnement Toulouse, GET UMR 5563, Toulouse, France.

7 <sup>2</sup>TOTAL S.A., Centre Scientifique & Technique Jean Féger, Pau, France.

8 <sup>3</sup>Sorbonne Université, CNRS-INSU, Institut des Sciences de la Terre Paris, ISTeP UMR 7193, F-75005 Paris,  
9 France.

10 <sup>4</sup>M&U sas, France.

11 <sup>5</sup>Institute of Geophysics, Ludwig-Maximilians-Universität München, Munich, Germany.

12 *Corresponding author:* Frédéric Mouthereau (frederic.mouthereau@get.omp.eu)

## 13 14 **Abstract**

15 The tectonic evolution of highly oblique continental margins that result from back-arc extension above lithospheric  
16 STEP faults is poorly understood. Here, we investigate the case of the Alboran margin in the eastern Betics  
17 characterized by crustal thinning of 15-10 km, oblique to the direction of slab retreat. The current deformation patterns  
18 indicate that oblique back-arc rifting is underway. However, it is unclear whether these conditions are those that  
19 prevailed during the formation of the metamorphic domes and intramontane basins. We review the temporal and  
20 spatial evolution of Neogene sedimentary basins and brittle deformation in the eastern Betics, and exploit offshore  
21 seismic reflection lines to propose a crustal-scale section across the oblique margin. The history of sediment infill and  
22 rates of subsidence combined with the analyses of fault slip data, confirm that brittle extension oriented from N20°E  
23 to EW occurred during an interval spanning from the Serravallian-early Tortonian to the late Tortonian (14-8 Ma).  
24 This extension is found associated with both normal and strike-slip regimes and the evolution of the strike-slip  
25 corridors flanking the metamorphic domes. The transtensional model forms a coherent scheme linking the ductile  
26 deformation associated with metamorphic domes and the formation of EW- and NW-SE/NNW-SSE-directed  
27 sedimentary basins in the brittle upper crust during the Tortonian. The oblique extension, which is closely associated  
28 with STEP faulting, occurred during the regional convergence between Africa and Iberia since the Miocene. Only  
29 recently, around 8 Ma, the slab detached, leading to local tectonic inversion. Such a type of narrow oblique rifted  
30 margin associated with transform-like plate boundaries is not unique but is expected to be hardly preserved in the  
31 geological record due to the transient nature of retreating subduction systems.



## 32 **1 Tear faulting and the formation of oblique transform margin in the Betics**

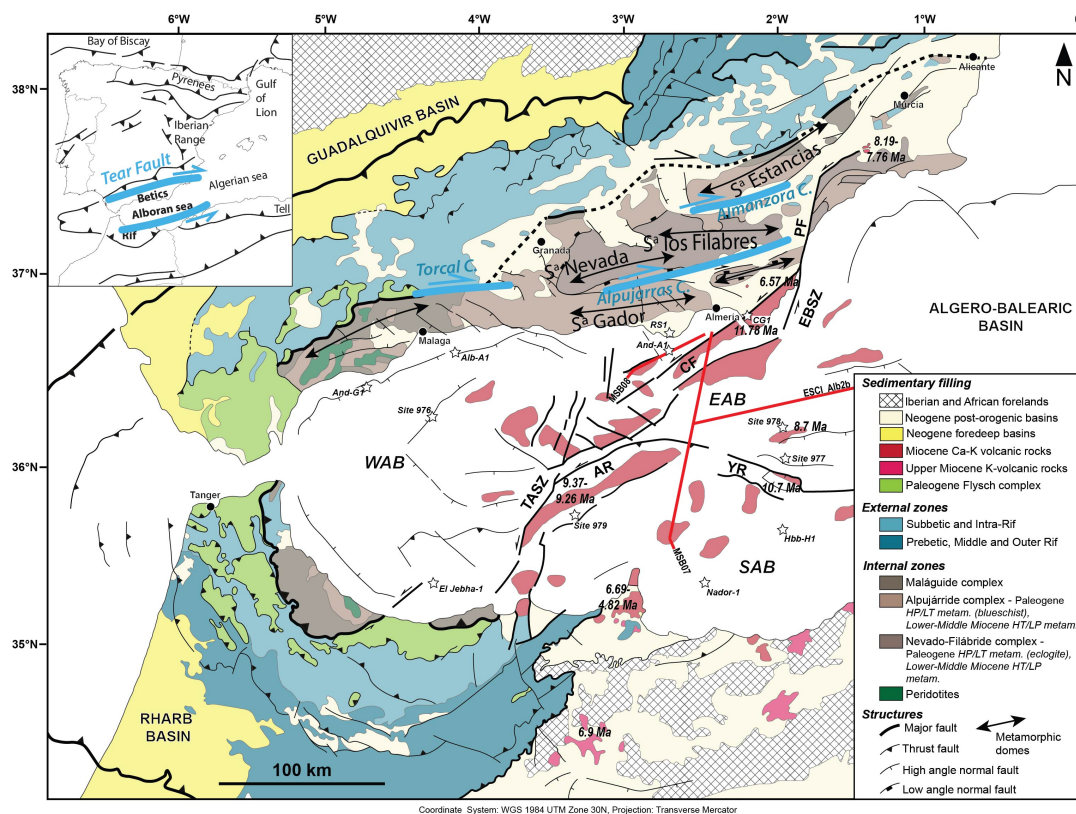
33 Lithospheric tear faults or subduction-transform edge propagator (STEP) faults are propagating strike-slip faults that  
34 accommodate the differential motion between the retreating subduction zone and the overriding back-arc plate (Govers  
35 and Wortel, 2005). Because of the relative motion between back-arc and surrounding plates, they are also propagating  
36 strike-slip faults defined by a sharp contrast in crustal thickness. As noted by Govers and Wortel (2005) such oblique  
37 fault boundaries do not necessarily form proper transform plate boundaries but broad zones of distributed deformation,  
38 accommodating differential trench-parallel extension, strike-slip motion and rotation. In case the lithospheric tear  
39 propagates within the continent-ocean transition, a narrow continental margin forms highly oblique to the direction of  
40 back-arc extension. This is documented, for instance, in the Carribean, along the transcurrent Carribean-South  
41 America plate boundary (Pindell and Kennan, 2009) or on the margin of the South Orckney microcontinent, along the  
42 Scotia-Antarctic plate boundary (Dalziel et al., 2013). Despite the large-scale kinematic picture is relatively well  
43 understood, there are only few places where continental crustal deformation associated with this peculiar type of slab-  
44 edge continental rift system can be studied.

45 Here, we focus on the Betic Cordillera, on the northern boundary of the Gibraltar arc (**Figs 1 and 2**). There, a rifted  
46 margin, defined by decreasing crustal thickness from 35 to 20 km in the Abloran basin (Diaz et al., 2016), is seen to  
47 develop above a STEP fault (Badji et al., 2014; Gallais et al., 2013; Jolivet et al., 2021a; Mancilla et al., 2015a). The  
48 tectonic expression of the transcurrent deformation during crustal extension above the lithospheric tear is however  
49 controversial. On the one hand, low-angle ductile extensional detachments with a top-to-the-west sense of shear are  
50 the main features accommodating deformation in the overriding plate. Yet, a-type metamorphic domes in the lower  
51 crust, elongated parallel to the E-W direction (**Fig. 1**), are viewed to express the transtensional deformation at the tip  
52 of propagating tear (Pourhiet et al., 2012). On the other hand, strike-slip faulting is interpreted as a late brittle  
53 deformation feature associated with E-W crustal strike-slip brittle faults between the metamorphic domes in the eastern  
54 Betics (Alpujarras corridor ; Sanz de Galdeano and Vera, 1992; Sanz de Galdeano et al., 1985; Martínez-Martínez et  
55 al., 2006) and in the western Betics (e.g. Torcal corridor ; Frasca et al., 2016) unrelated to ductile deformation (**Fig.**  
56 **1**). In line with the latter interpretation, the dextral motion these strike-slip faults accommodate is assumed to be  
57 modest, reflecting a recent post-8 Ma kinematic change that accompanies the end of slab retreat, and onset of  
58 compression in the Gibraltar Arc (Do Couto et al., 2014; d'Acremont et al., 2020; Jolivet et al., 2021a; Martínez-  
59 García et al., 2017).

60 The lack of structural, temporal constraints and quantification of belt-parallel motion along these faults indicates,  
61 however, that we do not yet fully understand their link with the long-term evolution of slab tearing and margin  
62 formation. For instance, the current deformation patterns brings critical evidence that both strike-slip faulting and  
63 extension operate synchronously, so that brittle strike-slip faulting and ductile extension might reflect the same  
64 tectonic episode. This is argued by ongoing extension illustrated by the west-directed GPS velocities increasing  
65 westwards, and the west-directed displacements increasing towards the Alboran domain revealing active right-lateral  
66 shear deformation (**Fig. 2**). The current transtensional deformation across the Betic Cordillera is also shown by the  
67 current stress regime defined by extension direction highly oblique (max. 20°) to the Betic structural trend (or 70°  
68 spanned by the direction of extension and normal of the rift trend). Right-lateral transtensional deformation in the



69 Betic agrees with evidence for west-directed lateral extrusion of the Alboran Basin (Borque et al., 2019; Palano et al.,  
 70 2015). In the east, the extrusion is accommodated by left-lateral strike-slip displacement along the Eastern Betic Shear  
 71 Zone (EBSZ; Borque et al., 2019), which is shaped by the Carboneras Fault (CF) and Palomerias Fault (PF). This fault  
 72 extends offshore, across the Alboran Sea, in the larger Trans-Alboran Shear Zone (De Larouzière et al., 1988; Stich  
 73 et al., 2006) moving at ~4 mm/yr, equivalent to the regional 5 mm/yr NW-directed convergence between Africa  
 74 (Nubia) and Europe (Fig. 2; Echeverria et al., 2013; Koulali et al., 2011; Nocquet, 2012; Palano et al., 2015, 2013;  
 75 Vernant et al., 2010). Here, we hypothesize that the present-day oblique extension patterns is at play since the Miocene  
 76 and explain the formation of the narrow Alboran rifted margin.  
 77

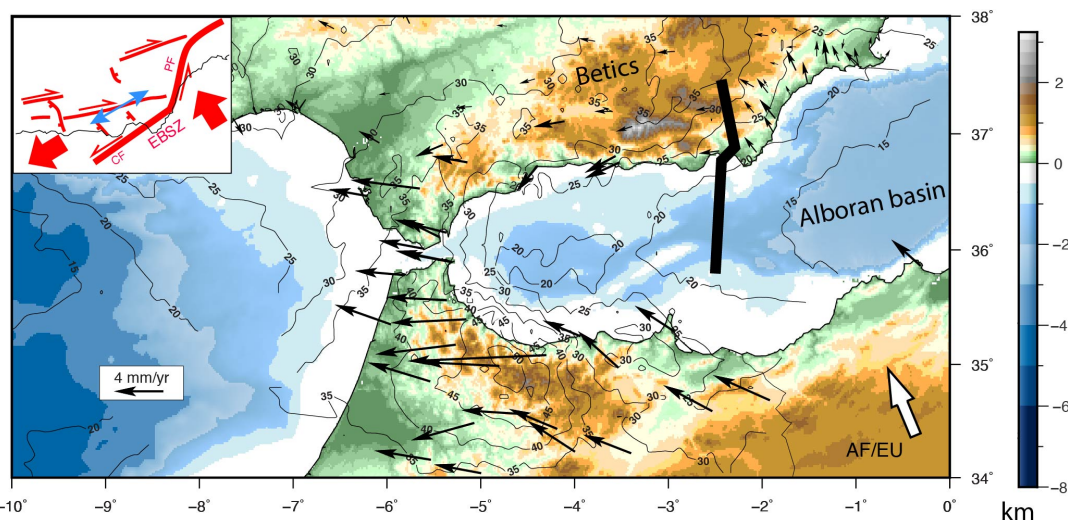


78  
 79 **Figure 1** : Geological map of the Betic-Rif arc. Main tectonic units and age of volcanism as well as major structures  
 80 and Neogene sedimentary basins are shown. The studied offshore seismic lines (red) is displayed as well as offshore  
 81 wells and ODP sites (★) for stratigraphic calibration in the East (EAB), South (SAB) and West Alboran basins  
 82 (WAB). CF: Carboneras Fault; PF : Palomerias Fault; AR: Alboran Ridge; YR: Yusuf Ridge; EBSZ : East Betic Shear  
 83 Zone; TASZ: Trans-Alboran Shear Zone.  
 84

85 Only recently high-resolution 3D numerical models have been able to predict the deep structure of oblique rift  
 86 domains. These models can be used as a guide to re-evaluate the evolution of the Betic region. 3D models by Jourdon  
 87 et al. (2021) predict that oblique extension results in narrow rifted margins, strike-slip faults and corridors coupled



88 with subsident pull-apart basins, normal faults and block rotations (**Fig. 3**). The recognition of block rotation in the  
89 Betic arc (Crespo-Blanc et al., 2016; Platzman, 1992), strike-slip corridors (**Fig. 1**) and NW-SE normal faulting, which  
90 defines extension direction highly oblique to the margin, (Galindo-Zaldivar et al., 2003; **Figs 1 and 2**) all support this  
91 view. The simulations of Jourdon et al. (2021) also show that the deeper ductile crust experiences thinning (vertical  
92 flattening) and stretching perpendicular to the strike of the margin in accordance with stretching lineations parallel to  
93 the metamorphic domes and low-angle detachments (**Fig. 3**). Other types of 3D numerical experiments show that  
94 sediment loading of strike-slip faults can result in asymmetric flexural basin with apparent normal fault throw  
95 (Neuharth et al., 2021) that can be mistakenly interpreted as resulting from orthogonal extension. Asymmetric basins  
96 are indeed intriguing characteristics of intramontane basins in the Betics (Augier et al., 2013; Do Couto et al., 2014).  
97 Although primarily found associated with divergent plate boundaries e.g. in the Gulf of California (Fossen et al., 2013;  
98 Fossen and Tikoff, 1998) highly oblique extension is also documented in active transform regions along the San  
99 Andreas Fault (Teyssier and Tikoff, 1998) or the North Anatolian Fault in Marmara Sea (Okay et al., 2004). A detailed  
100 analysis of highly oblique rifting deformation in the Gulf of California recognises similar tectonic elements as for the  
101 Betics, such as extensional detachment systems orthogonal to the divergence and upper crustal folds trending parallel  
102 to the divergence (Fossen et al., 2013).  
103



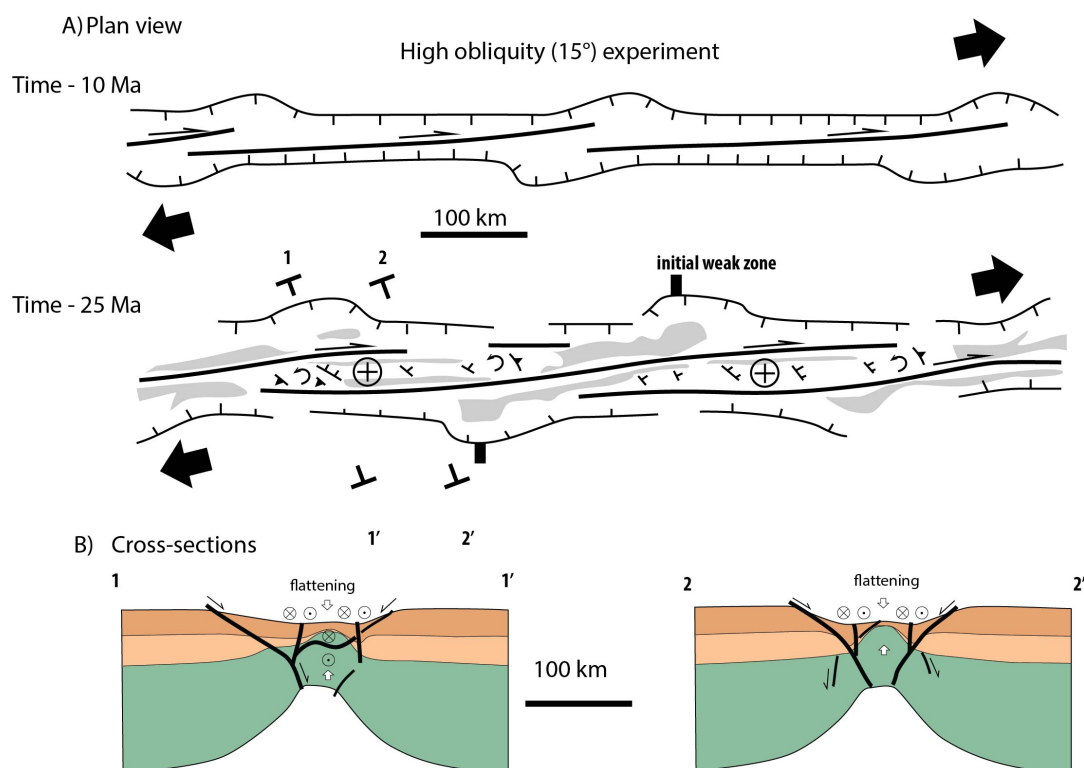
104 **Figure 2** : Present-day kinematics in the Betic-Rif arc and eastern Betic Cordillera (inset). GNSS-based displacements  
105 in the Alboran block and northern Africa shown in a fixed Eurasian reference frame (black arrows after Palano et al.,  
106 2015) are oblique to the AF/EU plate convergence (white arrow) inferred from plate tectonic Morvel model (Argus et  
107 al., 2011). Labelled contours depict the crustal depth given in kilometers as inferred from deep seismic profiles and  
108 receiver functions analysis (Diaz et al., 2016). In the eastern Betic (inset), W-directed stretching is taken up by EW-  
109 directed right-lateral strike-slip fault and NW-SE normal faults. Extension direction resolved from focal mechanisms  
110 (blue arrows) are after (Stich et al., 2006). CF : Carboneras Fault; PF : Palomeras Fault; AR : Alboran Ridge; YR :  
111 Yusuf Ridge; EBSZ : East Betic Shear Zone; TASZ : Trans-Alboran Shear Zone.  
112  
113

114 Several tectonic features need further discussion however. First, the relevance of strike-slip faulting in the past is  
115 debatable as only a few occurrence of crustal-scale strike-slip faults are mapped. Second, the detail of the temporal





116 and spatial relationships between the formation of the oblique/transform margin and STEP faulting remain elusive.  
117 We here review the temporal and spatial evolution of Neogene intramontane sedimentary basins and related brittle  
118 deformation in the eastern Betics. In addition, we exploit offshore seismic reflection lines to propose a new crustal-  
119 scale section across the oblique margin. Based on these constraints we present a tectonic scenario for the formation of  
120 the high-obliquity rift margin in back-arc setting controlled by STEP faulting.  
121



122  
123 **Figure 3** : Sketch showing two steps (after 10 Myrs and 24 Myrs) of a 3D thermo-mechanical model of oblique rifting  
124 in plan view (A) and cross-sections (B). Results are redrawn after (Jourdon et al., 2021) for the case of a highly oblique  
125 experiment where extension is set with an angle of 15° with respect to the rift axis. Grey regions in (A) are basins  
126 adjacent to uplifted domains (cross-circle symbol) associated with right-lateral strike-slip faults. Cross-sections (B)  
127 depict the abrupt crustal thinning that occur perpendicular. Crustal thinning is most visible for the lower crust and  
128 produces the formation of an abrupt necking domain controlled by rift-parallel normal faults dipping towards the  
129 center of the rift and right-lateral strike-slip faults.  
130

## 131 2. Geodynamics and STEP faulting in the Betics

132 The onset of N-directed movement of Africa, by the Late Cretaceous-Paleogene, led to a Laramide-like contraction  
133 from Morocco throughout Western Europe (Mouthereau et al., 2021). South of Iberia, in the Betic-Rif domain, the  
134 closure of hyper-extended rift systems and oceanic basins of the Atlantic-Alpine Tethys resulted in the development  
135 of a proto-Betic accretionary prism, likely largely submerged (Angrand and Mouthereau, 2021; Daudet et al., 2020;  
136 Vergés and Fernández, 2012). By about 50 Ma, the acceleration of plate convergence led to the shortening of

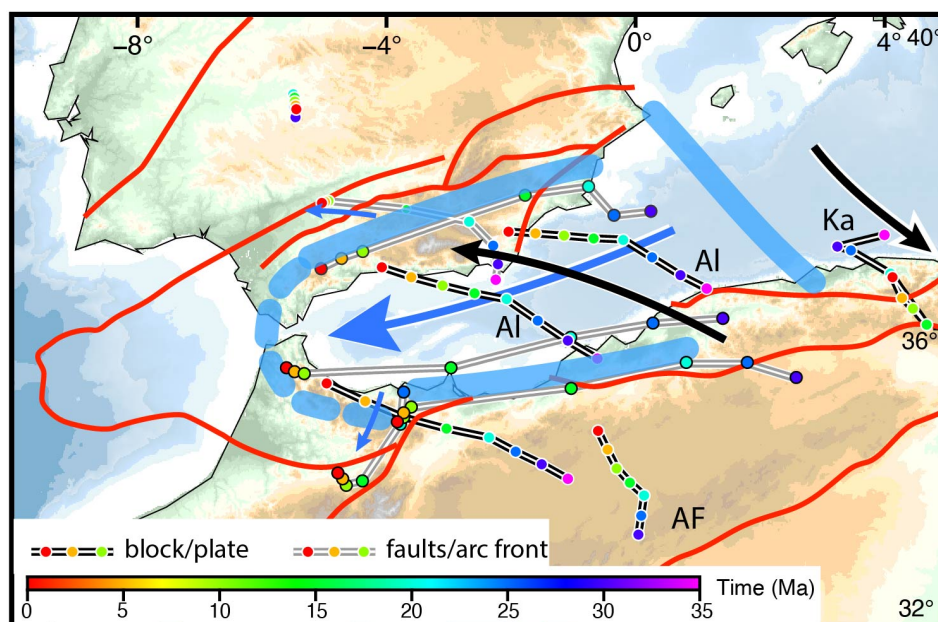


137 continental rift and oceanic basins and topographic uplift all over Iberia (Daudet et al., 2020; Mouthereau et al., 2021,  
138 2014; Rat et al., 2019; Vacherat et al., 2016; Waldner et al., 2021) associated with onset of continental rifting along the  
139 Western European Rift (e.g. Mouthereau et al., 2021). 35 Ma ago, as Africa convergence slowed down, the western  
140 Mediterranean sea opened accompanied by retreating slabs (Dewey, 1988; Dewey et al., 1989; Faccenna et al., 2014;  
141 Jolivet and Faccenna, 2000; Rosenbaum et al., 2002). Subduction occurred mainly before 30 Ma as argued by age  
142 constraints on high-pressure mineral assemblages (Romain Augier et al., 2005a; Bessi re et al., 2021; Booth-Rea et  
143 al., 2015; Gomez-Pugnaire and Fernandez-Soler, 1987; Platt and Vissers, 1989; Platt and Whitehouse, 1999) and has  
144 been suggested to last until the mid-Miocene in the eastern Betics e.g. (Platt et al., 2013). The timing of formation of  
145 the Alboran basin is constrained to 23 to 16 Ma by the oldest deposits found on Alboran basement and by the timing  
146 of high-temperature metamorphic overprint and rapid cooling to shallow crustal temperature (Bessi re et al., 2021;  
147 Daudet et al., 2020; Janowski et al., 2017; Johnson et al., 1997; Platt et al., 2005; Sosson et al., 1998; V zquez et al.,  
148 2011; Zeck et al., 1992).

149 All kinematic reconstructions agree that extension results from the westward migration of the arc front and retreat of  
150 the Alboran slab, well imaged below the Gibraltar arc as a steeply-dipping high-velocity anomaly (Bezada et al., 2013;  
151 Heit et al., 2017; Mancilla et al., 2018, 2015a, 2015b; Palomeras et al., 2014; Spakman and Wortel, 2004; Villase or  
152 et al., 2015). These reconstructions, however, differ according to the paleo-position of Alboran terrane, and hence to  
153 the amount and vergence of subduction (Angrand and Mouthereau, 2021; Hinsbergen et al., 2014; Lonergan and  
154 White, 1997; Romagny et al., 2020; Rosenbaum et al., 2002; Verg s and Fern ndez, 2012). Seismic tomography  
155 reveals that slab detachment and tearing occur along the conjugate Alboran margins of the southern Betics and  
156 northern Africa (Govers and Wortel, 2005; Heit et al., 2017; Mancilla et al., 2015a; Meighan et al., 2013; Spakman  
157 and Wortel, 2004).

158 In **Fig. 4** we refer to the reconstruction of Angrand and Mouthereau (2021) that has the advantage of reconciling  
159 previous western Mediterranean models (Romagny et al., 2020; Verg s & Fern ndez, 2012) with recent  
160 thermochronological analyses in western Betics (Daudet et al., 2020) and other geological data (see compilation in  
161 Mouthereau et al., 2021). This model accounts for the existence of an upper Cretaceous-Paleogene foreland basin that  
162 formed adjacent to a proto-Betic orogen. In this reconstruction about 400 km of slab retreat is estimated since about  
163 35 Ma (gray path, blue arrows in **Fig. 4**). It is worth noting that for Romagny et al. (2020) a similar amount (i.e. 400  
164 km) is accommodated by back-arc extension of the Alboran crust, implying the same magnitude of displacement along  
165 the STEP fault in the Betics. In the reconstruction of Angrand and Mouthereau (2021), however, crustal thinning in  
166 Alboran basin is linked to delamination retreat of the Alboran lithospheric mantle towards the west. In such a model,  
167 because of the decoupling between crust and mantle, the length of the delaminated slab resolved at depth in seismic  
168 tomography, should not be simply translated into the amount of crustal extension in the Alboran domain. This further  
169 implies the displacement across the STEP fault must be also less than 400 km. Daudet et al. (2020) suggested that an  
170 extension of 110 km estimated from the restoration of low-angle detachment systems in the central and eastern Betics  
171 (Mart nez-Mart nez et al., 2002) is likely to be a more accurate crustal estimate of the movement Alboran domain  
172 rather than the total slab length.

173



174

175

176

177

178

179

180

181

182

**Figure 4:** Kinematics of African plate (AF), Alboran (Al) and Kabyliides (Ka) blocks with respect to fixed European plate since 35 Ma reconstructed after Angrand and Mouthereau (2021). Thick blue lines depicts the position of lithospheric tear faults (between Al and Europe and Africa) and transfer faults (between Al and Ka). Black arrows indicate the regional movement of Al and Ka with respect to Europe along black motion paths presented from 35 Ma to present. Grey motion paths refer to the motion of specific structures relative to Europe, including the motion of the arc front (thick blue dashed line) and faults in red. Dark blue arrow depicts the movement of the arc front due to retreating delamination towards the west.

183

### 3. Miocene extension in the eastern Betics

184

#### 3.1 Relationships between domes and basins : from transtension and pure extension to late tectonic inversion

185

186

187

188

189

190

191

192

193

194

195

196

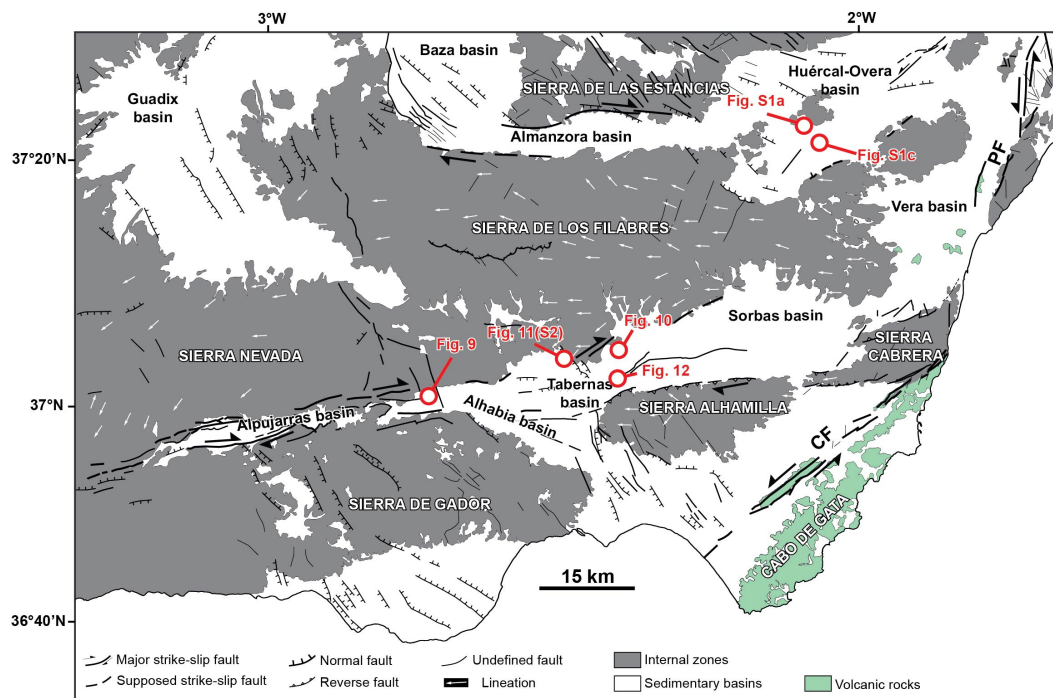
197

The most prominent extensional features in the eastern Betics are : 1) E-W elongated ranges that formed metamorphic domes with foliations bearing prominent E-W stretching lineations (**Fig. 5**; e.g. Sierra de los Filabres-Sierra Nevada, Sierra de Gador and the Sierra de las Estancias) and Serravallian-Tortonian sedimentary basins (Tabernas-Sorbas, Alpujarras, Almanzora and Huércal-Overa basins); 2) NNW-SSE/NW-SE normal fault systems and basins oblique to the domes such as the NW-SE trending Guadix-Baza and Alhabia basins (Galindo-Zaldivar et al., 2003; Martínez-Martínez and Azañón, 1997) (**Fig. 5**). They are described as asymmetric half grabens (Do Couto et al., 2014; Martínez-Martos et al., 2017; Pedrera et al., 2010, 2009) formed during the Upper Serravallian-Early Tortonian (Augier et al., 2005b; Augier et al., 2013; Meijninger and Vissers, 2006). Several of these NW-SE faults are active and cut across the metamorphic domes and the sedimentary basins (Augier et al., 2005a; Booth-Rea et al., 2004; Giaconia et al., 2012; Montenat and Ott d'Estevou, 1999).

In addition to these structures there are E-W right-lateral strike-slip faults that define structural corridors, like the Alpujarras corridor/basin between the Sierra de Gádor and the Sierra Nevada, and the Almanzora corridor/basin between the Sierra de los Filabres and Sierra de las Estancias (**Fig. 5**). The left-lateral Carboneras and Palomeras fault



198 system (Reicherter and Hübscher, 2006; Scotney et al., 2000) marks the tectonic limit with the Cabo de Gata volcanic  
199 province (Fig. 5).  
200 The domes are extension-related features interpreted either as 1) EW-metamorphic domes resulting from the  
201 exhumation in the footwall of a regional W-directed extensional low-angle detachments, later folded during post-  
202 Tortonian N-S contraction (e.g. Montenat & Ott d'Estevou, 1990; (Sanz de Galdeano and Vera, 1992; Sanz de  
203 Galdeano and Alfaro, 2004; Martínez-Martínez et al., 2002; Martínez-Martos et al., 2017; Pedrera et al., 2010, 2007)  
204 or 2) Miocene metamorphic domes formed by constrictional ductile strain regime accompanying W-directed  
205 stretching of the Alboran domain and trench retreat, with limited overprint by the Tortonian contraction ca. 8 Ma  
206 (Augier et al., 2013; Augier et al., 2005; Augier et al., 2005b; Galindo-Zaldivar et al., 2015; Jolivet et al., 2021b;  
207 Martínez-Martínez et al., 2002). Low-temperature constraints from the Nevado-Filabride and Alpujarride complexes  
208 confirm the west-directed exhumation of the basement that occurred progressively from the Sierra de los Filabres at  
209 ~13-11 Ma (Serravallian) in the East to the Sierra Nevada at 8-6 Ma (Tortonian) in the West (Clark and Dempster,  
210 2009; Janowski et al., 2017; Johnson et al., 1997; Platt et al., 2005; Reinhardt et al., 2007; Vázquez et al., 2011).  
211



212  
213 **Figure 5** : Tectonic map of the eastern Betics showing the main structural elements in black after Augier et al. (2005)  
214 and Do Couto (2014). CF: Carboneras Fault; PF : Palomeras Fault.  
215

216 Tectonic models for the formation of Neogene intramontane sedimentary basins vary depending on the prevailing  
217 tectonic regime. EW-directed basins have been early described as pull-apart basins (e.g Alpujarran corridor) (Sanz de  
218 Galdeano et al., 1985). Structural analyses then led to re-interpret these structures as transfer zones resulting from



219 differential extension between exhuming core-complexes (and detachment systems) since the Serravallian (13-11 Ma)  
220 later refolded during Tortonian (9-8 Ma) compression (Martínez-Martínez et al., 2006). In support to the dominant  
221 regional compressional stress regime, Martínez-Martos et al. (2017) proposed the E-W depressions are related to the  
222 tectonic reactivation of crustal weakness zone as dextral strike-slip faults in a counterclockwise rotation,  
223 accommodating part of the the N-S shortening. There are evidence that at the end of the Tortonian a regional uplift  
224 occurred, rising the remnants of late Tortonian marine platform, 7.2 Ma in age, to 1600 m above sea level in the Sierra  
225 de Gádor (Braga et al., 2003; Janowski et al., 2017), coincidently with the onset of contraction in the Sierra Alhamilla  
226 and Sierra de los Filabres (e.g. Do Couto et al., 2014), in the Alboran domain (e.g. (Martínez-García et al., 2017) and  
227 on the margins of the eastern Betic (Giaconia et al., 2013).

228 Based on the prevalence in some EW-trending basins, like the Huércal-Overa basin, of EW-trending normal faults,  
229 these basins have alternatively been interpreted as resulting from late exhumation stage of the domes, possibly as soon  
230 as the Serravallian, but mostly after the early Tortonian (syn-sedimentary faulting) (Augier et al., 2013; Romain Augier  
231 et al., 2005b; Meijninger and Vissers, 2006). The NW-SE/NNW-SSE sedimentary basins (Guadix, Baza, Alhabia;  
232 **Figs. 5**), in contrast, are extensional basins formed parallel to the direction of the regional compression (Sanz de  
233 Galdeano and Vera, 1992; Larouzière et al., 1988). E-W strike-slip corridors, aligned in the direction of the domes,  
234 and NW-SE normal faulting patterns are both key features consistent with predictions from models of oblique  
235 extension at transform margin (**Fig. 3**). Yet, based on existing structural and tectonic syntheses a clear temporal  
236 relationships between E-W ductile stretching in the domes and transcurrent deformation is not established (**Fig. 5**).

237

### 238 **3.2 Are the Tortonian rift-related subsidence consistent with oblique extension ?**

239 The stratigraphic architecture and depositional evolution of Tortonian intramontane basins provides first-order  
240 informations on the distribution of crustal thinning. The oldest sediments deposited unconformably on the Paleozoic-  
241 Triassic basement are red alluvial conglomerates and deltaic series dated from Serravallian to lower Tortonian (~11-  
242 9 Ma) (**Fig. 6a**). These continental deposits are thicker and well exposed on the flanks of the Almanzora basin and on  
243 the northern Huércal-Overa basin (HOB), compared to the Alpujarras Corridor (AC) and Tabernas basin (TB) (**Figs.**  
244 **6 and 7a**; Augier et al., 2013; Pedrera et al., 2010, 2007; Poisson et al., 1996).

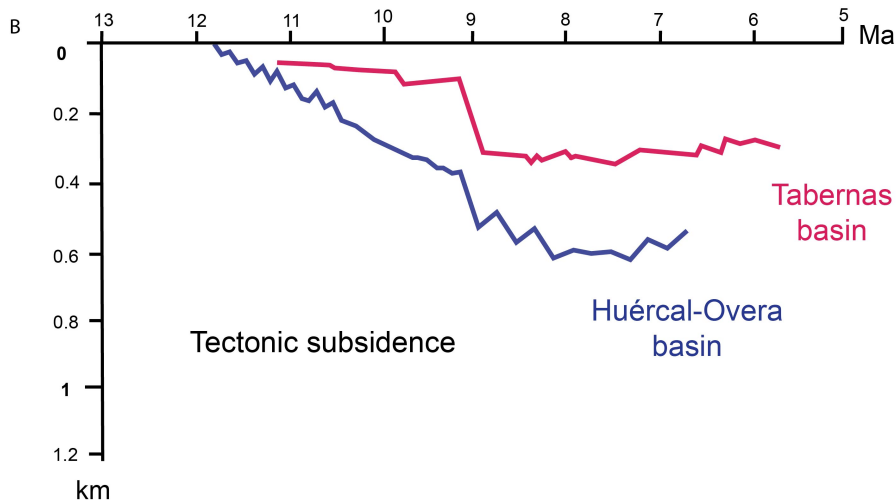
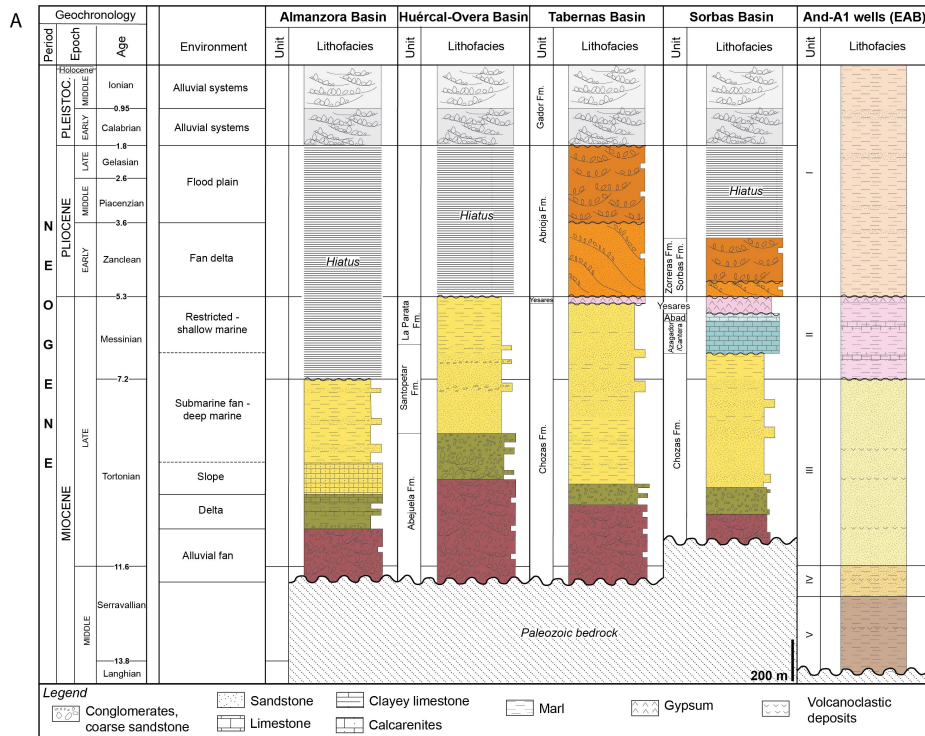
245 Paleogeographic reconstructions indicate they were deposited on a large emerged domain, stretching from Huercal-  
246 Overa to Granada, in the West and in Tabernas, to the South (Braga et al., 2003). Sourced from the Nevado-Filabride  
247 metamorphic complex (Hodgson and Haughton, 2004; Kleverlaan, 1989; Meijninger and Vissers, 2006; Pedrera et  
248 al., 2010, 2007; Pickering et al., 2001; Weijermars et al., 1985) these deposits mark the onset of surface exhumation  
249 of the Sierra de Las Estancias and Sierra de Los Filabres.

250 During this initial stage, HOB is the most subsident basin (**Figs. 6b, 7a and 7b**), accumulating sediments at rates of  
251 400 m/Ma while rates are 140-180 m/Ma in the Tabernas basin (**Fig. 6b**) (Augier, 2005). Higher subsidence in the  
252 HOB, which also started earlier than in other basins, suggests extension occurred originally to the North associated  
253 with the exhumation of the Sierra de Las Estancias. Basal continental conglomerates are overlain by grey coarse-  
254 grained Tortonian sandstones found occasionally, e.g. in the Almanzora basin, intercalated with marine marls (**Figure**





255 **6a**). They are topped by mid-Tortonian bioclastic calcarenite and coral reefs (Braga et al., 2003; Martin et al., 1989;  
256 Pedrera et al., 2007).  
257 During the same interval, TB recorded the deposition of 300 to 400 m of coarse to medium-grained deltaic marine  
258 clastics overlying unconformably the lowermost red series (**Fig. 6a**). These sediments pass upwards, e.g. in TB, to  
259 deeper marine 1200 m-thick turbiditic and marls series intercalated with regional-scale megabeds, revealing the onset  
260 of rapid tectonic subsidence (Haughton, 1994; Kleverlaan, 1989, 1987; Pickering et al., 2001; Weijermars et al., 1985).  
261 Details of depositional architecture of the Tortonian suggest that part of this subsidence evolution was controlled by  
262 E-W directed strike-slip faults (Haughton, 2000) under transtensional strain.  
263 The transition from continental to deep marine sedimentary environments (water depth of 400-600 m according to  
264 Poisson et al., 1999) witnesses the rapid rift-related tectonic subsidence achieved during the upper Tortonian times  
265 (~9 Ma; **Figs. 6** and **7c**) (Romain Augier et al., 2005b; Montenat and Ott d'Estevou, 1992; Weijermars et al., 1985).  
266 At around 8 Ma, accumulation rates drop by a factor of two to 200 m/Ma in HOB and 70 m/Ma in TB, revealing a  
267 marked reduction in subsidence. Subsidence then became negative as basement uplifted from around 7 Ma (**Figs. 6b**  
268 and **7d**) in both TB and HOB.  
269  
270



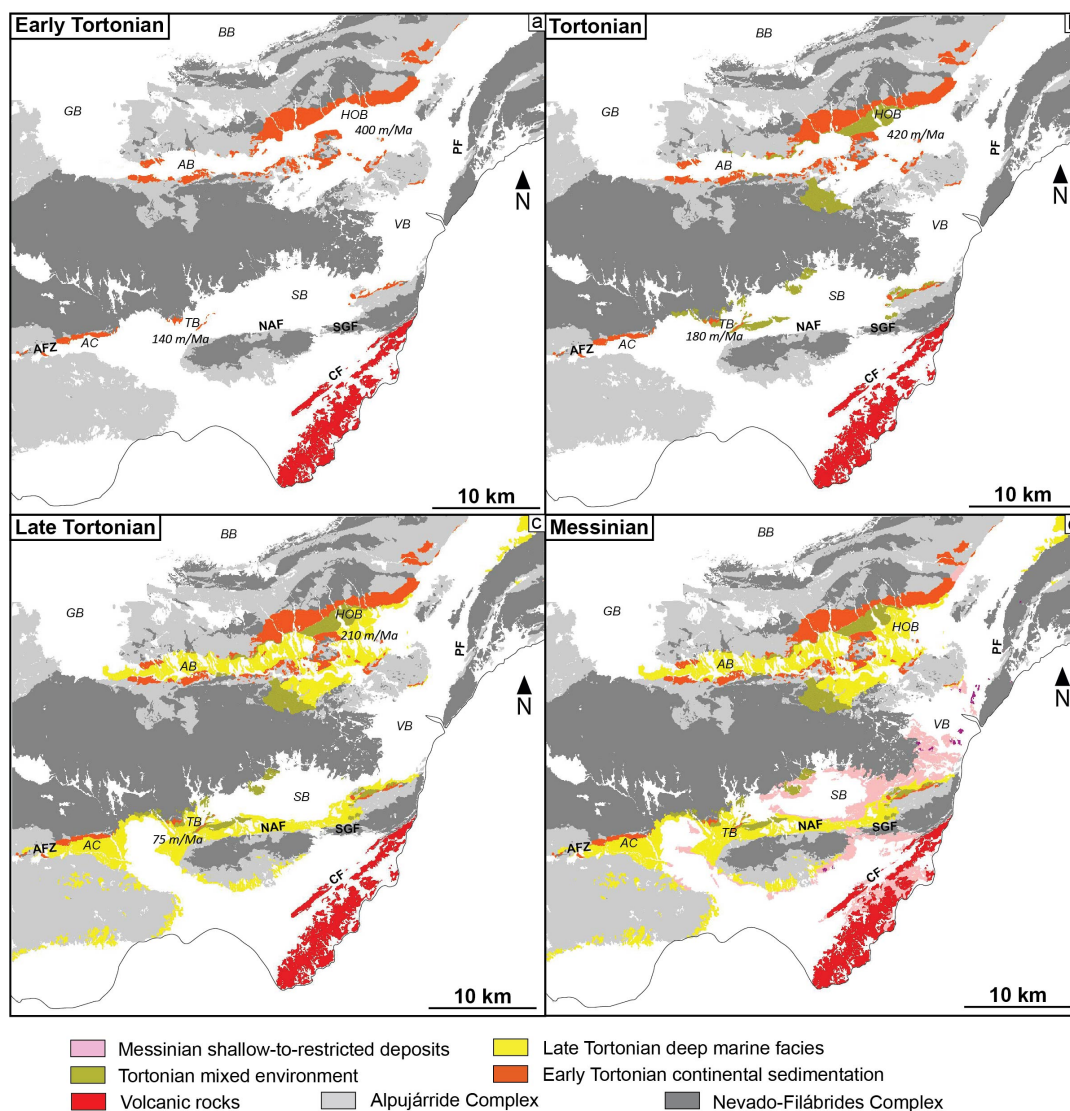
271 km  
 272 **Figure 6** : Stratigraphic evolution and lithologies of intramontane basins in the eastern Betics and offshore A1 well.  
 273 (a) Neogene stratigraphy and basin-fill correlation in the Almanzora and Huercal-Overa basins (Mora, 1993), Tabernas  
 274 basin (Hodgson and Houghton, 2004; Kleverlaan, 1989; Pickering et al., 2001) and Sorbas basin (Fortuin and  
 275 Krijgsman, 2003; Martin and Braga, 1994; Riding et al., 1998). Middle Miocene sedimentary environments in the  
 276 Alboran Sea are after (Comas et al., 1992). (a) Neogene tectonic subsidence evolution for Tabernas basin and Huércal-  
 277 Overa basin are from (Augier, 2004). The curves are obtained from backstripping techniques incorporating local  
 278 eustatic and paleobathymetric corrections.



279

280 The geometry of the Almanzora (Pedrera et al., 2009), Sorbas (e.g. Do Couto et al., 2014) and Huércal-Overa basin  
281 basins (Pedrera et al., 2010) inferred from gravity measurements indicate that these basins are asymmetrical and  
282 deepening southwards (**Fig. 5**). This sediment infill pattern recalls the formation of asymmetrical basins predicted by  
283 numerical models of flexural strike-slip basins (Neuharth et al., 2021). According to this model, the asymmetry  
284 observed should reflect the development of strike-slip basins loaded by sediments originated from the North. In  
285 addition, a larger subsidence in HOB is an indication of abrupt crustal thinning to the south of Sierra de las Estancias  
286 where the crustal thickness of 35 km is the largest (**Fig. 2**). Therefore, at least the Serravallian-Tortonian infill patterns  
287 agree with oblique extension.

288



289  
 290  
 291  
 292  
 293  
 294

**Figure 7:** Distribution of (a) lower Tortonian, (b) Tortonian, (c) upper Tortonian and (d) Messinian deposits based on geological mapping of the different basins. CF: Carboneras Fault; PF : Palomeras Fault; SGF: South Gafarillo fault; NAF: North Alhamilla fault; AFZ: Alpujarras fault zone; BB: Baza basin; GB: Guadix basin; AB: Almanzora basin; HOB: Huercal-Overa basin; VB: Vera basin; SB: Sorbas basin; TB: Tabernas basin; AC: Alpujarras corridor.

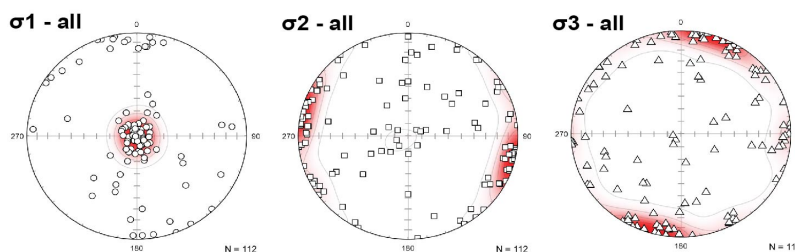
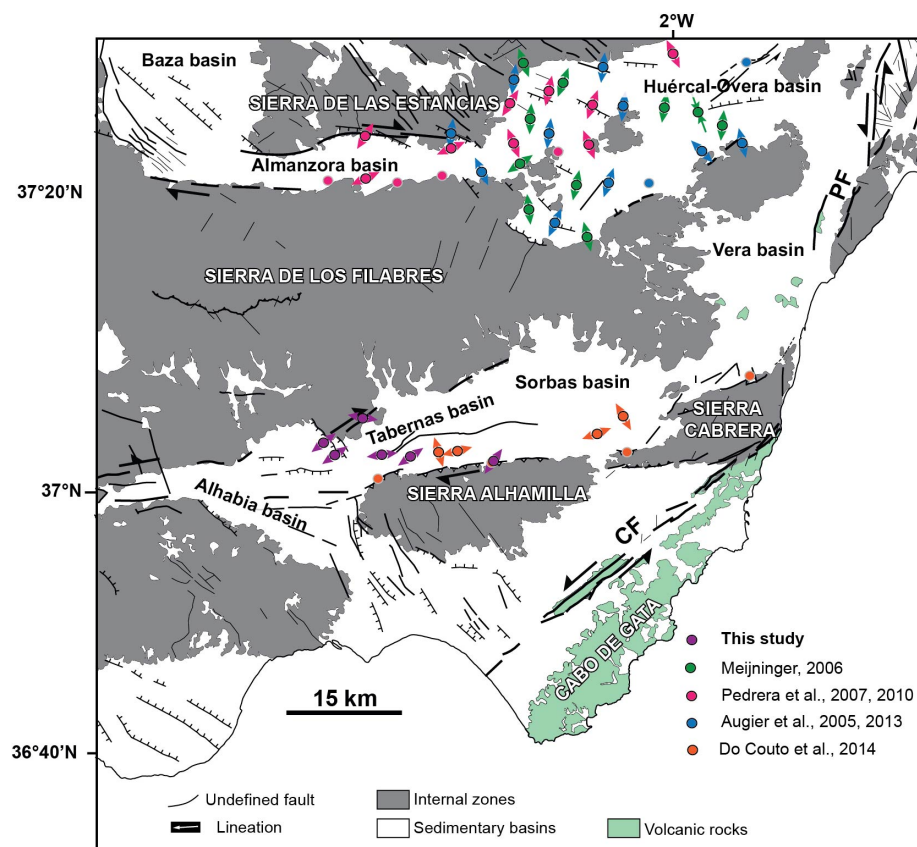
#### 295 4. Brittle faulting : pure extension versus transtensional deformation in Neogene basins

##### 296 4.1. Tectonic regime in the eastern Betics

297 **Figure 8** presents a compilation of 112 fault slip data inversion previously analysed in the eastern Betics combined  
 298 with new measurements conducted in the Alpujarras Corridor and in the Tabernas basin (**Table S1**). Most faults are  
 299 syn-Tortonian or cut through the Tortonian. This compilation emphasizes a regional trend of  $\sigma_3$  stress axes oriented



300 NNE-SSW (N20°E) with subordinate  $\sigma_3$  oriented E-W. In details, this well-defined regional horizontal extension  
 301 reflects a combination of pure normal faulting regime ( $\sigma_2$  horizontal and oriented NW-SE/WNW-ESE) and strike-  
 302 slip faulting regime ( $\sigma_2$  vertical to steeply-dipping and  $\sigma_1$  horizontal an striking NNW-SSE). N-S to NW-SE  
 303 compression is also reported in the HOB associated with incipient synform and depocenter which is dated to the lower  
 304 Tortonian coeval with the prominent EW/WSW-ENE extension (e.g. Pedrera et al., 2010).  
 305 We describe below, based on a selection of outcrops in the vicinity of the contact between Tortonian basins and major  
 306 metamorphic domes, the expression of EW and NW-SE extensional faulting in the field. We then discuss how they  
 307 are linked to the regional stress regimes.  
 308



309





310 **Figure 8:** Synthesis of stress regimes resolved from fault slip data inversion in Tortonian basins. Color-coded circles  
311 with arrows depict tectonic sites where extension (given as arrows) is horizontal (pure extensional or strike-slip stress  
312 regimes). Sites where reverse tectonic regimes prevail are shown as circles highlighted in grey. Below, stereoplots of  
313 paleostresses  $\sigma_1$ ,  $\sigma_2$  and  $\sigma_3$  show a compilation of all brittle tectonic regimes extracted from Table S1. Collectively  
314 they define a prominent extension oriented NNE-SSW with a subordinate E-W-striking extension. CF: Carboneras  
315 Fault; PF : Palomerias Fault.

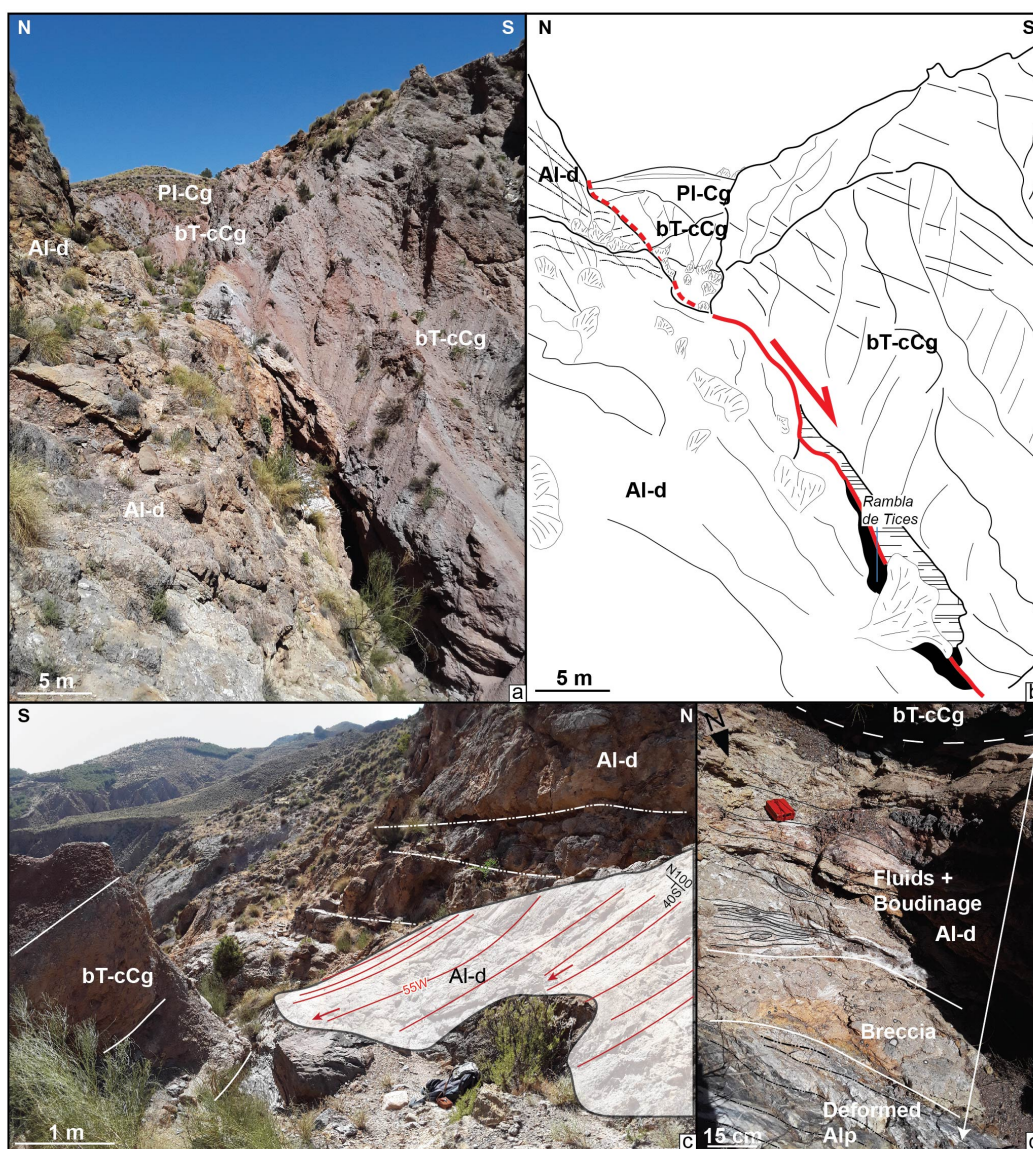
316

#### 317 **4.1 EW-directed faulting: evidence for pre-Tortonian oblique extension ?**

318 In Tortonian intramontane basins, one of the main set of faults is represented by E-W-directed faults, including ENE-  
319 WSW to ESE-WNW sets. North of the Alpujarras Corridor (AC), 3 km to the NE of Canjáyar, the contact between  
320 the basal Tortonian conglomerates and the series of Alpujarride complex is exposed in the Rambla de Tices. It is  
321 shaped by a 2-meter thick fault zone (**Figs. 9a,b**) striking N100°E, which has a normal sense of slip with a right-lateral  
322 strike-slip component (**Fig. 9c**). It consists of cataclastic breccias and sheared blocks (boudins) of the host rocks (**Fig.**  
323 **9d**). This major fault is found along the 65 km-long Alpujarras fault zone described by Martínez-Martínez (2006) as  
324 a major strike-slip dextral transfer zone south of the Sierra Nevada that accommodates both WSW-extension and dextral  
325 movement. It is mechanically consistent with NE-SW/ENE-WSW extension under a strike-slip regime as resolved  
326 nearby along the same faults system (Martínez-Martínez, 2006). **Fig. 9** indicates the fault is parallel to the basal  
327 Tortonian series but cuts across the Alpujarride complex. In the HOB, on the southern flank of the Sierra Limaria, the  
328 unconformity between the lower Tortonian red conglomerates and the Alpujarride units (Rambla de Cordoba, 2km  
329 NW Arboleas, **Figs. S1a, b**) is found reactivated as a normal fault with a dextral shear component.

330 To the North of TB, a large morphological surface presents a rare exposure of the micaschist basement of the Nevado-  
331 Filabrides complex allowing the study of deformation on the southern flank of the Sierra de los Filabres (**Fig. 10**). The  
332 deformed NF series shapes a kilometric-size antiform with axial planar surface dipping towards the North. The steeply-  
333 dipping cleavages directed NE-SW on its southern flank are deformed by numerous dextral shear zones with lengths  
334 ranging from 100 m to less than 5 m (**Fig. 10b, c**). In addition to isoclinal folds parallel to the main foliation that are  
335 clearly associated to an early stage of ductile EW-stretching, we recognize close to the strike-slip shear zones, steeply-  
336 dipping metric-size open to tight folds inclined to the NE (**Fig. 10d**). To the south, Tortonian conglomerates are  
337 overlying unconformably the folded NF foliation. This stratigraphic relationships and the average low dip of Tortonian  
338 strata (20°SE) indicate that strike-slip deformation occurred before the deposition of Tortonian conglomerates and  
339 after the tilting of the NF foliation (see cross section in **Fig. 10a**). This argues that the transition from W-directed  
340 ductile extension in the metamorphic domes known to have started in the Burdigalian and the right-lateral strike-slip  
341 faulting occurred around the Langhian-Serravallian (13-14 Ma). This interval is often considered to mark the transition  
342 from ductile to brittle extension (e.g. Augier et al., 2013). Because strike-slip faulting postdates folding of the NF  
343 foliation, and are consistent with WSW-ENE oblique extension, we suggest that the Sierra de los Filabres metamorphic  
344 dome formed in a transtensional strain regime. This hypothesis conforms with prediction of transtension at the tip of  
345 the STEP fault (Le Pourhiet et al., 2012) and with model of oblique extension (see **Fig. 3**).

346



347  
 348 **Figure 9.** (a) and (b) Fault zone at the contact between the Tortonian basal conglomerates and the series of the  
 349 Alpujarride complex south of AC (Rambla de Tices, see Fig. 5 for location). (c) slickensides on the fault zone reveals  
 350 a normal sense of slip with right-lateral strike-slip component found in association with (d) cataclastic breccias,  
 351 sheared boudins of metamorphic and sedimentary rocks. Al-d: Alpujarride dolomites; bT-cCg: basal Tortonian  
 352 continental Conglomerates; PI-Cg: Pliocene Conglomerates. Coordinates 37.031944°N/-2.716274°E.  
 353

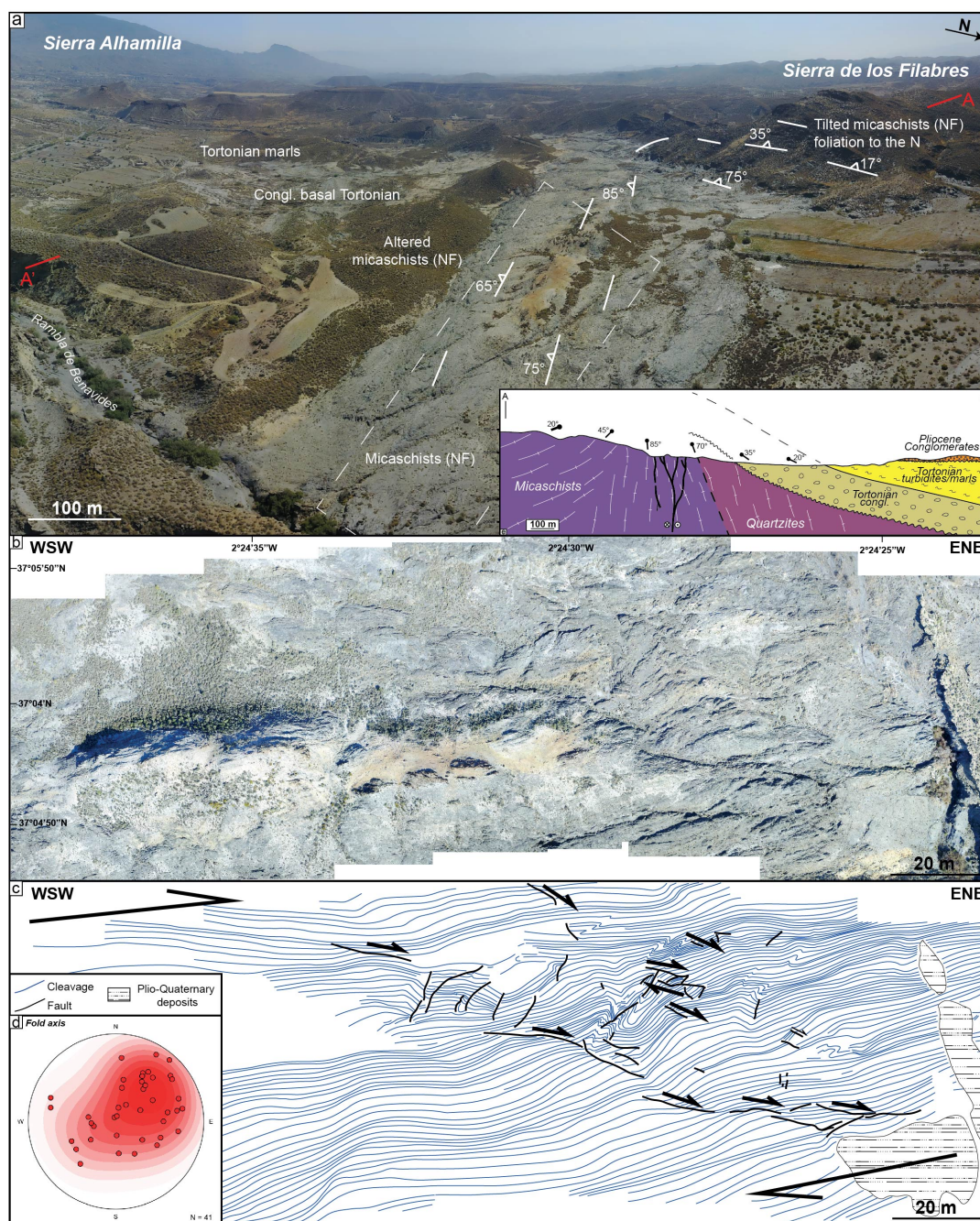
354 **4.1.2. NW-SE-directed normal faulting**

355 A second set is represented by NW-SE directed normal faults (Fig. 8). They are found, for instance, on the border of  
 356 the NW-SE Alhabia basin, where they cut across the basement and interrupt the westward continuity of the Sierra de



357 los Filabres. One major fault zone of this system is well exposed in the Arroyo del Verdelecho, 7 km to the west of  
358 Tabernas, on the eastern border of the Alhabia basin (**Figs. 11 and S2**). From a regional point of view this large NW-  
359 SE fault zone controls the deepening of the Tortonian basin and the position of Pliocene depocenter in its hangingwall,  
360 towards the West. NW-SE normal faults also cut across the lower Tortonian conglomerates in the hanginwall but their  
361 throw diminishes upward in the upper Tortonian margin sediments, suggesting fault activity during the late Tortonian  
362 (**Fig. 11**). One major fault zone is outlined by cataclastic breccias made of marbles originated from the exhumed  
363 Alpujarride complex in the Sierra de los Filabres (**Fig. S2**).  
364 South of HOB (south of Arboleas), NW-SE faults are seen cutting through the late Tortonian sands and marls series,  
365 indicating that NE-SW extension is at least Tortonian (**Figs. S1c, d**).  
366





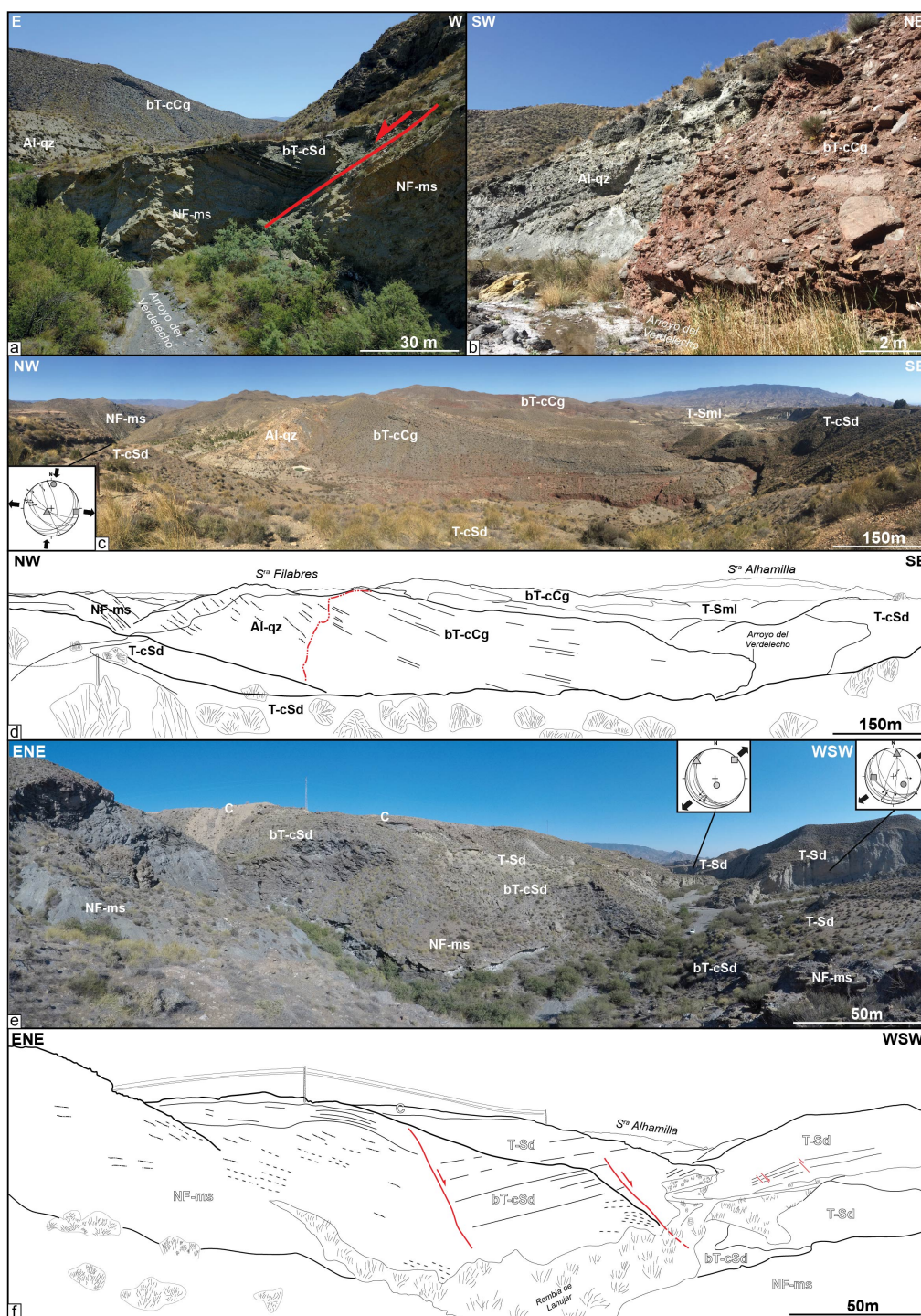
367  
 368  
 369  
 370  
 371  
 372

**Figure 10** : (a) Drone view taken in the SSW direction of the southern flank of the Sierra de los Filabres at the contact with the Tabernas basin (see Figure 5 for location). Local folding of the micaschist is apparent in the right where the foliation is striking NNE-SSW and is dipping  $\sim 25^\circ$  E whereas it is vertical and striking SW-NE in the center of the studied area forming paleosurface. Local cross section highlights the unconformable contact between the Tortonian conglomerates and overlying on the basement. (b) High-resolution drone images of the paleosurface and (c) line-



373 drawing of the foliation revealing secondary folding (see **(d)** stereoplot of fold axes inclined to the NE) and dextral  
374 shear zones. Coordinates 37.082777°N/-2.410544°E.  
375  
376  
377



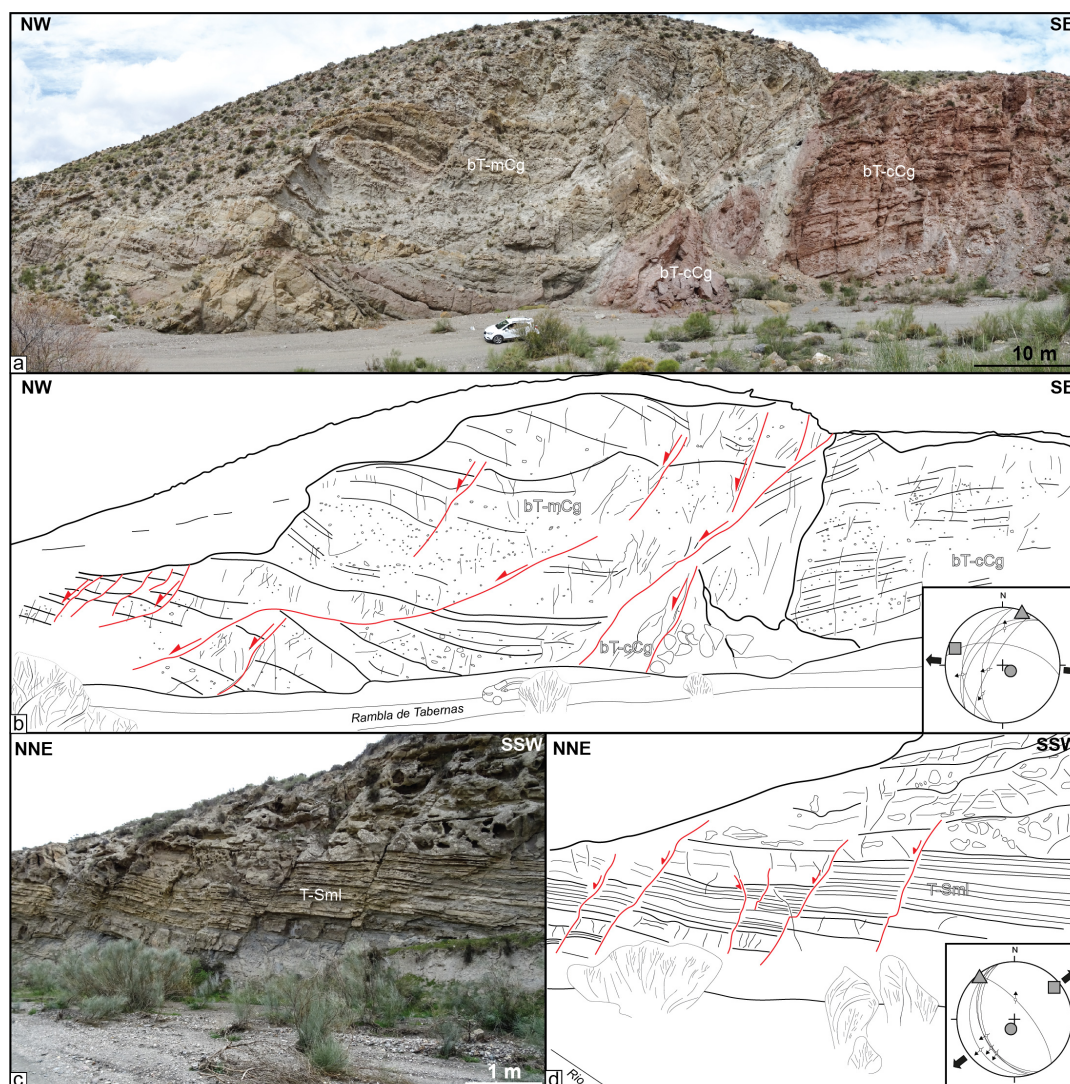




379 **Figure 11** : (a) Field photographs of a NW-SE normal fault at the contact between the Nevado-Filabride micaschists  
380 (footwall) and Tortonian sediments (hangingwall). (b) Stratigraphic contact between grey and red basal Tortonian  
381 continental conglomerates. These thick Tortonian series rest conformably on the Alpujarride complex (c, d).  
382 Coordinates 37.059507°N/-2.478386°E. (e, f) NW-SE Normal faults cutting across the NF micaschists basement.  
383 These faults that also affect the early Tortonian deposits are sealed by late Tortonian deposits and are therefore syn-  
384 depositional. See Figure 5 for location. Al-qz: Alpujarride quartzites; NF-ms: Nevado-Filabride micaschists; bT-cCg:  
385 basal Tortonian continental Conglomerates; bT-cSd: basal Tortonian continental Sandstones; T-cSd: Tortonian coarse  
386 Sandstones; T-Sd: Tortonian Sandstones; T-Sml: Tortonian Sandstones-marls; C: calcretes. Coordinates  
387 37.061279°N/-2.490309°E. Paleostress orientations are in Table S1.  
388

389 Both fault slip data and our own observations argue for a regional pre-Tortonian and syn-early Tortonian NNE-  
390 directed extension. This direction of extension is also found associated with less well-developed strike-slip regimes  
391 (Fig. 8). It is consistent with the D1-D2 phase of brittle deformation found in HOB (Augier et al., 2013). The fact that  
392 extension and strike-slip regimes occurred synchronously, or overlap rapidly in time, supports the view that they  
393 reflect the same large-scale tectonic setting. The reason why strike-slip faulting is less apparent in the field than  
394 expected in models in Fig. 3 is likely to reflect the fact that oblique extension is not fully partitioned between normal  
395 and strike-slip components and is actually distributed along oblique structures. Moreover, where strike-slip faults are  
396 found they are associated with narrow corridor basins or near the contact between the cover and basement but not in  
397 the center of HOB or TB. The NNE-SSW to NW-SE faults appear to postdate the deposition of the early Tortonian  
398 red conglomerates and is synchronous with the deposition of marine Tortonian series (Fig. 12). These normal faults  
399 currently form half-graben filled with Plio-Quaternary deposits (Guadix, Baza, Alhabia) and are active today. But the  
400 importance of extension-related brittle deformation over brittle compression decreases eastwards. Indeed, a late brittle  
401 compressional event oriented roughly N-S is described in the literature as a D3 brittle event (e.g. in HOB) associated  
402 with reverse and strike-slip faults (Augier et al., 2013). The post-late Tortonian shortening is seen responsible for fold  
403 amplification and reverse faulting on the northern limb of Sierra de Alhamilla and Sierra de los Filabres, and locally  
404 in the eastern part of the HOB near the termination of left-lateral strike-slip faulting evolution of the Alhama de Murcia  
405 fault (Fig. 8).





406

407 **Figure 12:** (a, b) N-S to NNE-SSW-oriented normal to dextral faults affecting the basal Tortonian continental  
408 conglomerates (bT-cCg) and marine conglomerates (bT-mCg) (Rambla de Tabernas). They form a long and tight E-  
409 W anticlinal crosses the Tabernas basin (see Figure 5 for location). (c, d) Several normal faults observed in Tortonian  
410 sandstones and marls (T-Sml). They are mostly oriented NNW-SSE. Coordinates 37.041648°N/-2.399318°E.  
411 Paleostress orientations are in Table S1.

#### 412 5. N-S crustal-scale section across the oblique/transform margin of Alboran basin

413 To examine further the structural relationships between extension and strike-slip faulting across the Alboran margin,  
414 we explore 2D multichannel seismic lines acquired during the MARSIBAL 1-06 cruise (Comas and MARSIBAL1-  
415 06 Scientific Party, 2007) and ESCI cruises (Comas et al., 1995) across the Eastern Alboran basin (EAB). The studied  
416 seismic dataset consists of ~300 km and are deep-penetration multichannel seismic reflection studies (12 s two-way  
417 travel time - TWTT). Here, we study two lines namely MSB08 and MSB07 (see location in Fig. 1). For stratigraphic



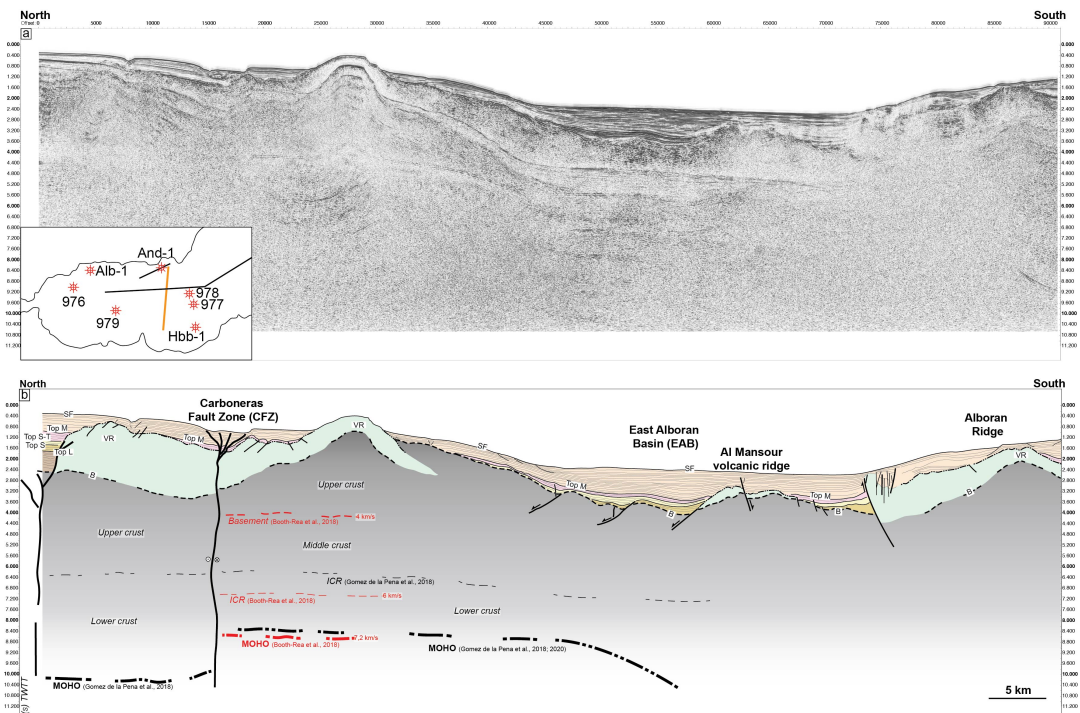
418 and structural correlations between the studied seismic lines, we used the Andalucía-A1 well (**Fig. 6a**) and results  
419 from ODP 977 and 978 legs (see location in **Fig. 1**). MSB08 is striking N70°E, slightly oblique to the shoreline. It is  
420 close, and runs parallel, to TM08 line of (Peña et al., 2018). It is calibrated by Andalucía-A1 well and ESCI-Alb1 line  
421 (Comas et al., 1995). Line MSB07 stretches in the N-S direction between the EAB in Spain and SAB to the north of  
422 Morocco parallel to line TM09 (Peña et al., 2018) and crosscuts line ESCI Alb2b presented in Comas et al. (1995)  
423 and Booth-Rea et al. (2007) (**Fig. 1**).

424

### 425 5.1 Offshore structures and stratigraphic architecture

426 The Carboneras Fault is well imaged north of MSB07 (**Fig. 13**). It forms a positive crustal-scale antiformal flower  
427 structure related to left-lateral strike-slip faulting that involves a Moho depth variation between 12 s to 9-8 s TWT  
428 after Gomez de la Peña et al. (2018). It separates a thin continental crust to the North (25-20 km; **Fig. 2**), from the  
429 magmatic calc-alkaline arc crust of the EAB with a thickness of 18 km in the south (Booth-Rea et al., 2007, 2018;  
430 Gomez de la Peña et al., 2018, 2020a).

431



432

433 **Figure 13** : Seismic reflection line MSB07 (location on **Fig. 1**). Discontinuous intracrustal reflectors (ICR) imaged  
434 between 3 and 6.5 s TWT, have been interpreted as mylonitic zones within the metamorphic basement (Carbonell et  
435 al., 1998; García-Dueñas et al., 1994; Gomez de la Peña et al., 2018). VR: Volcanic Ridge; B: Acoustic basement;  
436 Top L : Top Langian; Top S: Top Serravallian; Top S-T: top Serravallian-Tortonian; Top M: Top Messinian; SF:  
437 Seafloor.

438

439

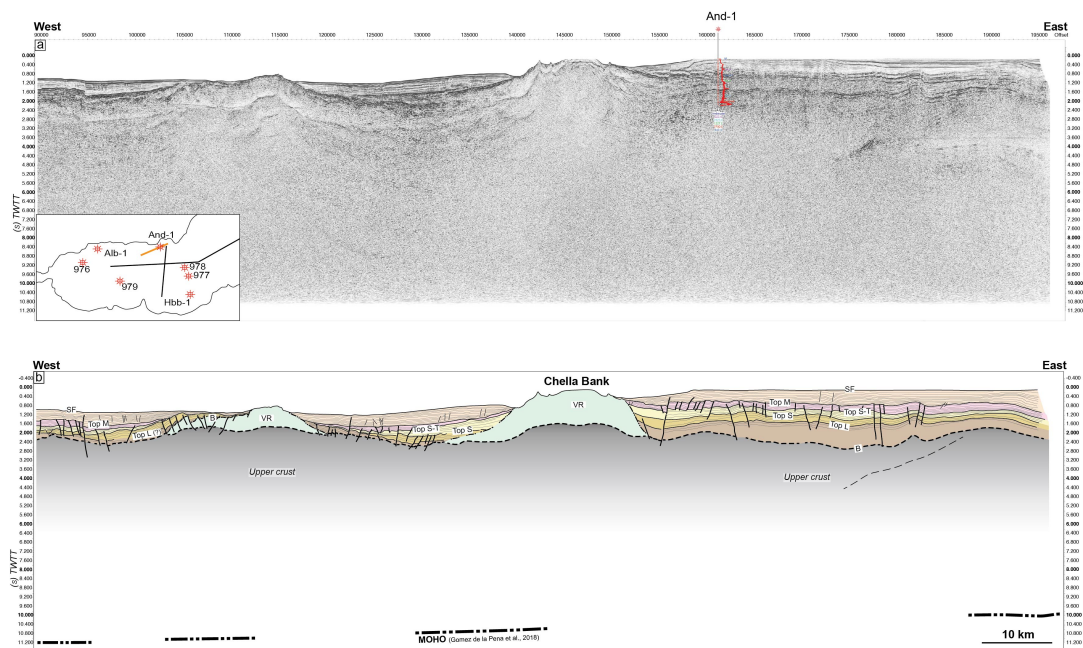


440  
441 Reflection seismic data (**Figs. 13, 14, 15**) collectively show a relatively well stratified crust, corresponding to the  
442 sediment cover, down to 2.4-4 s TWT which outlines the acoustic basement with high reflectivity (B). Locally, the  
443 top basement reflector coincides with erosional palaeo-relief or high angle normal faults bounding basement highs.  
444 These faults are oriented mostly NW-SE to NE-SW and cut across the basement. We recognized on seismic images  
445 magmatic additions in the continental crust that are shaped by volcanic edifices exposed on the seafloor (e.g. Chella  
446 Bank) or slightly buried (Alboran Ridge) outlined by symmetric downlaps and onlaps of sediments. These  
447 constructions form topographic highs such as the Chella Bank on the MSB08 line (**Fig. 14**), the Alboran Ridge on the  
448 MSB07 line (**Fig. 13**) and the Maimonides Ridge on the ESCI-Alb2b line (**Fig. 15**). All the reflectors corresponding  
449 to layers as old as Tortonian are onlapping against the volcanic ridges confirming that the volcanic activity occurred  
450 during the middle to late Miocene times, which is otherwise shown by Duggen et al. (2008). Some reflectors up to the  
451 top Messinian (top M) onlap onto the volcanic ridges probably as a result of Pliocene uplift.  
452 The stratigraphy offshore, on the continental crustal domain, is defined by the recognition of five seismic stratigraphic  
453 units in Andalucia-A1 well (Jurado and Comas, 1992) labeled I-V from top to base (**Figs 6 and 16**) and separated by  
454 unconformities. The seismostratigraphic units I to V vary in thickness (**Fig. 16**) and their architecture is conditioned  
455 by the occurrence of basement highs and crustal-scale faults.  
456 Below the Miocene sedimentary filling, Andalucia-A1 well reveals ~190m of phyllitic and quartzitic meta-sediments  
457 (2.4 to 4 s TWT below the Alboran basin, **Figs. 13 and 14**) topped by Langhian to Tortonian marls (top at ~1.6 to 3.4  
458 s TWT below the Alboran basin) interbedded with Tortonian-Messinian tuffs and basaltic lavas. These units have  
459 been correlated in the magmatic arc crust of EAB after Gomez de la Peña et al. (2020b). The older deposits (Unit V)  
460 Langhian-Serravallian in age, consist of clays and marls with intercalated sands and volcano-clastic deposits. The  
461 seismic facies of this Unit V is made of moderate amplitude and low frequency discontinuous reflections packages  
462 (Figure 18), and is only present in the Northern Alboran Basin. They are correlated with volcanic series in the EAB  
463 (vY3) (Gomez de la Peña et al., 2020b). They pass upward into Serravallian sand-silty clay turbidite (Unit IV) possibly  
464 correlated with volcanic series in EAB (vY2 after Gomez de la Peña et al., 2020b). This unit exhibiting low to moderate  
465 amplitude, moderate frequency drawing continuous sheeted to disrupted reflectors, is unconformably overlying Unit  
466 V and locally onlaps onto the basement. Thickness of Unit IV remains rather thin in the North and East Alboran Basin.  
467 It can't be properly identified in the South Balearic Basin, east of the Maimonides volcanic ridge (**Fig. 15**). The Unit  
468 III dated from late Serravallian to late Tortonian is represented by sandstones interbedded with volcano-clastic levels  
469 which correlates in EAB with volcanics vY1 unit. Unit III contains internal reflections characterized by low to moderate  
470 amplitude, moderate frequency continuous sheeted reflectors. Its thickness remains relatively constant from the NAB  
471 to the EAB, and is identified beneath the Messinian Unit II in the South Balearic Basin. Unit II corresponds to the  
472 Messinian evaporite, carbonate, volcanic, and volcanoclastic deposits interbedded with fine-grained sediments and is  
473 equivalent to unit III of (Peña et al., 2020b) in EAB. Seismic facies of Unit II is marked in the Alboran domain by  
474 lower amplitudes and lower frequency reflectors. In ESCI-Alb2b line, Unit II increases drastically east of the  
475 Maimonides ridge, which delimits the western boundary of the salt deposits in the Western Mediterranean basin during  
476 the Messinian Salinity Crisis (Haq et al., 2020). Unit II is topped by Unit I made of Pliocene to Quaternary clays and





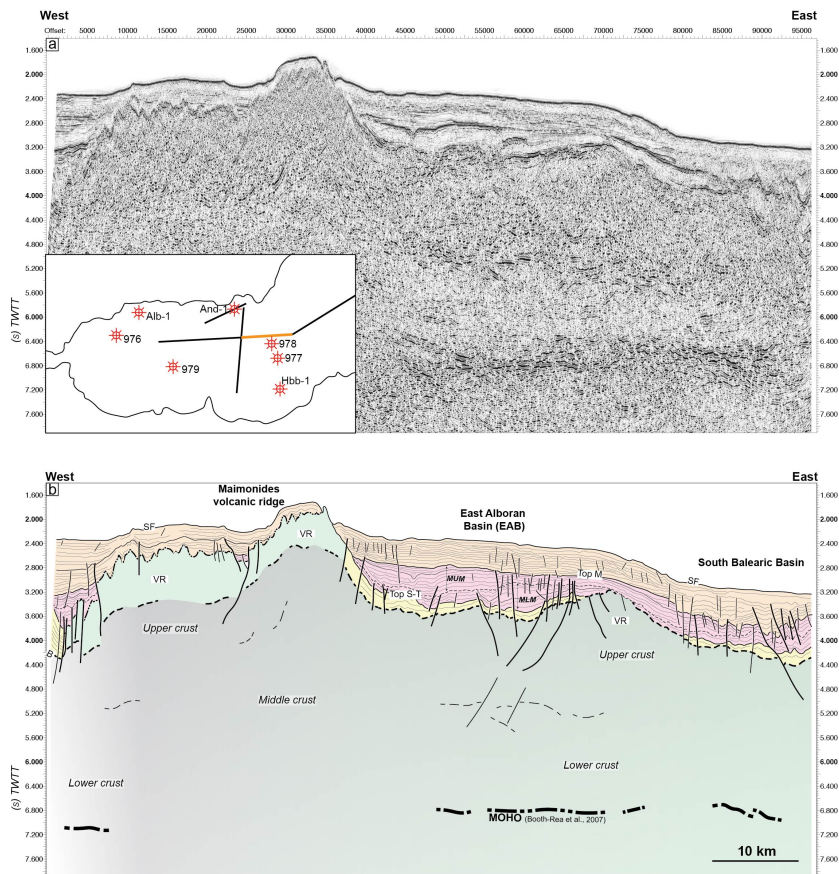
477 sanstones, which are correlated with units II and I in EAB (Gomez de la Peña et al., 2020b). Unit I is marked by thinly  
478 bedded, mostly parallel, high-frequency and low amplitudes reflectors (**Fig. 18**). Its thickness fluctuates in response  
479 to sedimentary processes (Juan et al., 2016).  
480 Along line MSB08 (**Fig. 14**) the Langhian-Serravallian (Unit V) is maximum 1600 m-thick (using a P-wave velocity  
481 of 3.2 km/s calculated within Andalusia-A1 well. In EAB, south of Carboneras Fault Zone, the total thickness of Unit  
482 V is only ~300 m on MSB07 (**Fig. 13**) and is absent in ESCI-Alb2b (**Fig. 15**). The Serravallian-Tortonian (Unit IV-  
483 III) interval shows only very limited sediment accumulation (~300 m) except near the NW-SE oriented normal faults  
484 where growth geometries are visible. These normal faults are sealed by the Tortonian-Messinian deposits, indicating  
485 a syn-sedimentary faulting during the middle Miocene (**Fig. 13**). With respect to offshore observations this  
486 sedimentary infill is more continuous and is also much thinner compared to TB and HOB where they are represented  
487 by thick conglomerates and marls/turbidites (> 1km) (**Fig. 7**), and they are eroded or not deposited along the axes of  
488 the metamorphic domes. The Messinian deposits (Unit II) are ~150-350 m-thick north of CF (MSB07-08 ; **Figs. 13**,  
489 **14**) and increase to about 1200 m eastward in the eastern EAB (ESCI-Alb2b ; **Fig. 15**), and in Algero-Balearic basin  
490 (Gomez de la Peña et al., 2020b). The top Messinian reflector is topped by thick horizontal sedimentary strata, with a  
491 maximum thickness of 1.2 s TWT (~2.4 km assuming a velocity of 2 km/s) on line MSB07, suggesting an important  
492 channel system during the Pliocene.  
493 The Pliocene-to-Quaternary series are poorly deformed except in the vicinity of CF and near the Alboran Ridge where  
494 this is associated with south-dipping reverse fault (**Fig. 13**). This late and still active compressional tectonics is  
495 revealed by the overthrusting of the SAB over the south margin of the EAB e.g. (Martínez-García et al., 2011).  
496



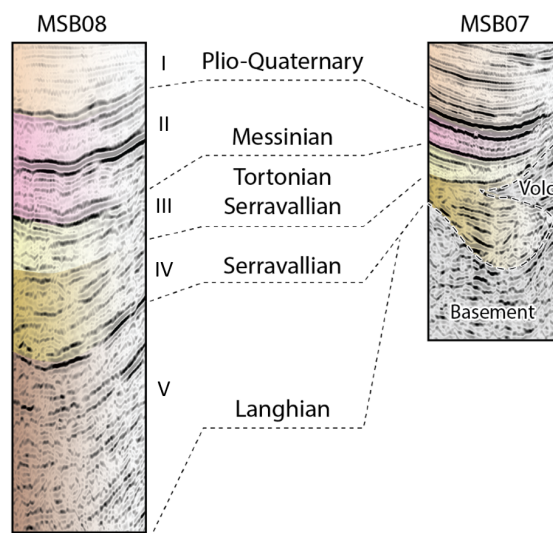
497



498 **Figure 14** : Seismic reflection line MSB08 (see location on **Fig. 1**). See Figure 13 for abbreviations. See also Figure  
499 S3 showing a zoom on the main seismic facies recognized in Andalucia-A1 well.  
500



501 **Figure 15. (a, b)** Seismic reflection line ESCI-Alb2b and interpretation (see Figure 1 for location). Seismic units are  
502 correlated with those defined by Booth-Rea et al. (2007). See Figure 13 for abbreviations.  
503  
504  
505

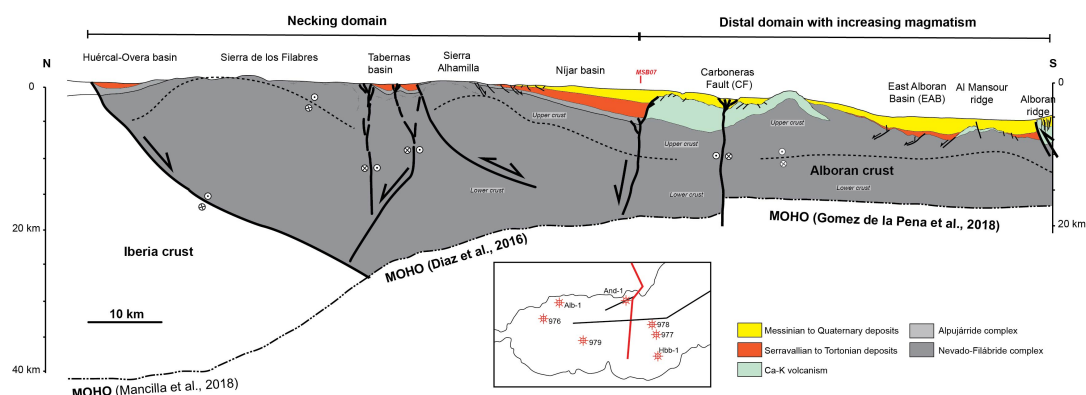


506

507 **Figure 16** : Seismic facies of units I to V seen through seismic lines MSB08 close to the shoreline and the line  
508 MSB07, located deeper in the East Alboran Basin.

### 509 **5.2 N-S crustal cross-section of the Alboran margin accounting for strike-slip faulting**

510 Based on subsurface constraints and field data, we have built a crustal cross-section across the rifted margin from the  
511 Sierra de las Estancias and Huerca-Overa basin (HOB), which represents the proximal margin, to the center of the  
512 Alboran margin (**Fig. 17**). The proximal margin is defined by a 30-35 km-thick crust. It preserves part of the thickness  
513 acquired during former orogenic phase that has been little involved in crustal thinning. The onset of crustal thinning  
514 to the south is recorded by the formation of strongly subsident and asymmetric basins of the HOB and TB, shaping  
515 the upper neck domain. This domain is characterized by orthogonal and oblique extension during the Tortonian  
516 accommodated by normal and strike-slip faulting. This boundary also corresponds to the position of the major STEP  
517 fault documented by seismology. From the Sierra de los Filabres to the south, the crustal thickness reduces to 25 km  
518 in the Tabernas basin along the Alpujarras strike-slip corridor and below the Sierra Alhamilla. The Nijar basin depicts  
519 the transition towards offshore distal domains with a crustal thickness of 20 km. The Tortonian and Messinian marine  
520 sediments are also thicker and a number of volcanic bodies accompany crustal thinning. Crustal thinning appears  
521 localized along the Carboneras Fault (CF), which juxtaposed crust with different crustal thickness (**Fig. 19**). South of  
522 CF, the crust thickness reduces below 20 km and shows increasing magmatic additions making the magmatic arc crust  
523 of the EAB (Gomez de la Peña et al., 2018 ; 2020). Interestingly, normal faulting in the EAB is sealed by middle-  
524 upper Tortonian deposits. Crustal deformation then shifted to the north in the CF and EBSZ strike-slip fault zones and  
525 to the south along the Alboran Ridge where reverse faulting occurred.



526  
527  
528  
529  
530  
531  
532

**Figure 17.** Crustal-scale cross section of the Alboran margin in the eastern Betics interpreted based on onshore and offshore constraints presented in the text. Note that in the necking domain the extension of faults downwards to Moho depths is not imaged on the seismics and therefore largely inspired by inferences from 3D numerical models (see Fig. 3).



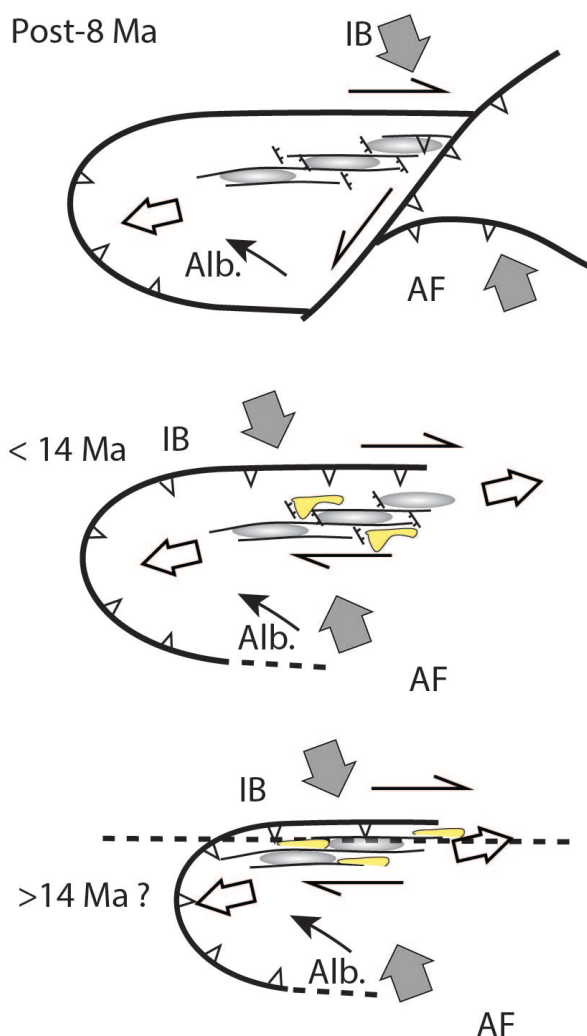
533 **7. Implications**

534 The question of whether the Miocene tectonic evolution of the Betics reflects crustal thinning associated with oblique  
535 back-arc rifting as suggested from present-day strain patterns is unclear in the literature. Back-arc extension, recent  
536 tectonic inversion and STEP faulting are generally considered to result from separated processes. We found based on  
537 a comparison between numerical models and analyses of basin evolution, fault kinematics and structure of the margin  
538 in the eastern Betics compelling evidences that crustal thinning occurred under oblique extension and was not  
539 restricted to the post-Tortonian evolution. Rather, oblique rifting possibly operated since at least the middle Miocene,  
540 as the slab retreat started in the Alboran basin and is therefore kinematically associated with STEP faulting.

541 One of the most striking tectonic feature of the Alboran margin (**Fig. 17**) is the abrupt N-S crustal thinning, from 35-  
542 30 km to 25-20 km, oblique to the direction of slab retreat. The history of sediment infill and rates of subsidence in  
543 intramontane basins (**Figs. 6 and 7**) combined with the analyses of fault slip data, confirm that brittle extension  
544 oriented from N20°E to EW occurred during an interval spanning from the Serravallian-early Tortonian to the late  
545 Tortonian (14-8 Ma). This extension is found associated with both normal and strike-slip regimes. In more details,  
546 these data suggest that N20°E extension is more represented in HOB, while the ENE-WSW to EW extension is found  
547 related with the evolution of the Almanzora corridor, Alpujarras corridor and Tarbenas basin flanking the metamorphic  
548 domes (**Table S1**). There are additional evidence that EW-directed dextral strike-slip faulting did occur during the  
549 Tortonian to the South and West of the HOB and represents this main phase of basin subsidence. These large-scale  
550 faults are later cut by Tortonian NW-SE faults that argue for more recent EW extension. Therefore, we infer that the  
551 domain south of the HOB, which also corresponds to a thinnest crust, has experienced transtensional deformation and  
552 EW extension.

553





554

555 **Figure 18:** Tectonic model of the evolution of the northern margin of the Alboran Rift. Large grey and white double  
556 arrows depict shortening, which is parallel to the AF/IB convergence, and the highly oblique extension, respectively.  
557 The thin black arrows is showing the motion of Alboran relative to Iberia (IB) taken from Figure 4. Half arrows  
558 depicts the distributed strike-slip faulting in the Betics. NW-SE directed normal fault and strike-slip basins (yellow)  
559 are consistent with the oblique extension. Grey-shaded ellipses represent the metamorphic domes.  
560

561 Several key specific tectonic features found in the eastern Betics are predicted by 3D models of oblique extension  
562 (**Figure 3**). Those include the E-W trending faults that are prevalent on the upper neck domain (i.e. Sierra de las  
563 Estancias and HOB), and E-W strike-slip faults (Almanzora and Alpujarras corridor) and NW-SE normal faults that  
564 are found associated with more distal domains where crustal thinning is the highest. Brittle E-W-directed stretching  
565 and dextral transcurrent deformation started in the Langhian-Serravallian (14-13 Ma). Tectonic inversion seems, in  
566 contrast, to have been increasingly more important when approaching the Carboneras and Palomeras strike-slip faults  
567 in the East since the late Tortonian.



568 According to temporal constraints, ductile thinning may have occurred between 23 to 16 Ma prior to brittle faulting  
569 at 14-13 Ma (**Figure 18**). The late/post-Tortonian times marks a change in the tectonic evolution of the region (Jolivert  
570 et al., 2021a; Mouthereau et al., 2021; Rat et al., 2022) as the mantle slab eventually detached and is responsible for  
571 Ca-K magmatism at 11-7 Ma (Duggen et al., 2008, 2004), compression and tightening of the metamorphic domes  
572 associated with the formation of the the EBSZ.

573 The strike-slip deformation model has the advantage to explain N-S crustal thinning in the Betics while back-arc  
574 extension is oriented E-W, in a continuum of deformation from the Miocene to the present. In this model, ductile  
575 stretching and ductile detachment associated with the development of the domes are the expression of oblique E-W  
576 extension. This provides a coherent scheme linking the formation of EW-directed basins in the brittle field associated  
577 with strike-slip faulting, and NW-SE/NNW-SSE sedimentary basins (Guadix, Baza, Alhabia) formed in transtension  
578 during the Tortonian. As such, the oblique extension, which is closely associated with STEP faulting required by slab  
579 retreat, is overall a characteristic feature of the regional NW-SE/NNW-SSE convergence since at least the Miocene.  
580 Only recently, around 8 Ma, as the slab detached, shortening started to prevail in the vicinity of the EBSZ (**Figure**  
581 **18**). As convergence was under way during oblique back-arc extension, high-pressure metamorphism and subduction  
582 possibly occurred during the mid-Miocene as argued in eastern Betics (Platt et al., 2013). Moreover, the case of  
583 exhumation of high-pressure rocks in oblique convergence setting associated with near-parallel orogeni extension is  
584 documented in other active orogen like Taiwan (Conand et al., 2020).

585 This highly oblique northern Alboran margin differs from typical transform fault margin such as those associated with  
586 the Atlantic ocean because it accommodates variations in intra-plate extensional movements, triggered by slab roll-  
587 back not variations in spreading rates. Strike-slip faults may have originated as low-angle normal which were later  
588 reactivated as thrusts during margin inversion. Similar observations, including metamorphism, strike-slip faulting,  
589 high geothermal gradients and volcanism has been made in Seram, north of the Banda Arc, which represents an other  
590 example of extremely thinned crust formed perpendicular to the direction of the slab retreat (Pownall et al., 2013).  
591 Such a narrow rifted margin associated with lithospheric STEP fault defines a class of oblique (and transform) margin  
592 that is expected to be hardly preserved in the geological record due the transient nature of retreating subduction  
593 systems.

594

595 **Data availability.**This study is based on data compilation. Data used in this study can be found in the appropriate  
596 references. Paleostress tensors obtained by the inversion of fault slip data are available online in the Supplement.

597

598 **Supplement.**The supplement related to this article is available on-line at:

599

600 **Competing interests.**The authors declare that they have no conflict of interest.

#### 601 **Authors contribution**

602 ML and FM, conceptualize, prepared figures and tables, compiled and interpreted field structural data and wrote the  
603 paper. DC provided and interpreted the seismic lines, reviewed the text and contributed to the writing. AJ carefully



604 examined the implementation of his numerical results and reviewed the text. EM, SC and VM, supervised and  
605 coordinate the different project tasks and reviewed the text.

606 **Acknowledgments**

607 The stereogram results were obtained using Win-Tensor, a software developed by Dr. Damien Delvaux, Royal  
608 Museum for Central Africa, Tervuren, Belgium (Delvaux and Sperner, 2003). The processed seismic data were  
609 interpreted using Kingdom IHS Suite© software. This research benefited from discussions and support of OROGEN  
610 project, an academic-industry research consortium between TOTAL, CNRS and BRGM.

611

612



## 613 References

- 614 Angrand, P., Mouthereau, F., 2021. Evolution of the Alpine orogenic belts in the Western Mediterranean region as  
615 resolved by the kinematics of the Europe-Africa diffuse plate boundary. *Bsgf - Earth Sci Bulletin*.  
616 <https://doi.org/10.1051/bsgf/2021031>
- 617 Argus, D.F., Gordon, R.G., DeMets, C., 2011. Geologically current motion of 56 plates relative to the no-net-  
618 rotation reference frame. *Geochemistry, Geophysics, Geosystems* 12. <https://doi.org/10.1029/2011gc003751>
- 619 Augier, R., 2004. Evolution tardi-orogénique des Cordillères Betiques (Espagne) : apports d'une étude intégrée 1  
620 vol., [II]-400 p.
- 621 Augier, R., Agard, P., Monié, P., Jolivet, L., Robin, C., Booth-Rea, G., 2005. Exhumation, doming and slab retreat in  
622 the Betic Cordillera (SE Spain): in situ  $^{40}\text{Ar}/^{39}\text{Ar}$  ages and P–T–d–t paths for the Nevado-Filabride complex.  
623 *Journal of Metamorphic Geology* 23, 357–381. <https://doi.org/10.1111/j.1525-1314.2005.00581.x>
- 624 Augier, Romain, Booth-Rea, G., Agard, P., Martínez-Martínez, J.M., Jolivet, L., Azañón, J.M., 2005a. Exhumation  
625 constraints for the lower Nevado-Filabride Complex (Betic Cordillera, SE Spain): a Raman thermometry and  
626 Tweequ multiequilibrium thermobarometry approach. *Bulletin de la Societe Geologique de France* 176, 403–  
627 416. <https://doi.org/10.2113/176.5.403>
- 628 Augier, R., Jolivet, L., Couto, D.D., Negro, F., 2013. From ductile to brittle, late- to post-orogenic evolution of the  
629 Betic Cordillera: Structural insights from the northeastern Internal zones. *Bulletin De La Société Géologique De*  
630 *France* 184, 405–425. <https://doi.org/10.2113/gssgfbull.184.4-5.405>
- 631 Augier, Romain, Jolivet, L., Robin, C., 2005b. Late Orogenic doming in the eastern Betic Cordilleras: Final  
632 exhumation of the Nevado-Filabride complex and its relation to basin genesis. *Tectonics* 24, n/a-n/a.  
633 <https://doi.org/10.1029/2004tc001687>
- 634 Badji, R., Charvis, P., Bracene, R., Galve, A., Badi, M., Ribodetti, A., Benaissa, Z., Klingelhoefer, F., Medaouri,  
635 M., Beslier, M.-O., 2014. Geophysical evidence for a transform margin offshore Western Algeria: a witness of a  
636 subduction-transform edge propagator? *Geophys J Int* 200, 1029–1045. <https://doi.org/10.1093/gji/ggu454>
- 637 Bessière, E., Jolivet, L., Augier, R., Scaillet, S., Précigout, J., Azañón, J.-M., Crespo-Blanc, A., Masini, E., Couto,  
638 D.D., 2021. Lateral variations of pressure-temperature evolution in non-cylindrical orogens and 3-D subduction  
639 dynamics: the Betic-Rif Cordillera example. *Bsgf - Earth Sci Bulletin*. <https://doi.org/10.1051/bsgf/2021007>
- 640 Bezada, M.J., Humphreys, E.D., Toomey, D.R., Harnafi, M., Dávila, J.M., Gallart, J., 2013. Evidence for slab  
641 rollback in westernmost Mediterranean from improved upper mantle imaging. *Earth and Planetary Science*  
642 *Letters* 368, 51–60. <https://doi.org/10.1016/j.epsl.2013.02.024>
- 643 Booth-Rea, G., Martínez-Martínez, J.M., Giaconia, F., 2015. Continental subduction, intracrustal shortening, and  
644 coeval upper-crustal extension: P-T evolution of subducted south Iberian paleomargin metapelites (Betics, SE  
645 Spain). *Tectonophysics* 663, 122–139. <https://doi.org/10.1016/j.tecto.2015.08.036>
- 646 Booth-Rea, G., Ranero, C.R., Grevemeyer, I., 2018. The Alboran volcanic-arc modulated the Messinian faunal  
647 exchange and salinity crisis. *Scientific reports* 8, 13015. <https://doi.org/10.1038/s41598-018-31307-7>
- 648 Booth-Rea, G., Ranero, C.R., Martínez-Martínez, J.M., Grevemeyer, I., 2007. Crustal types and Tertiary tectonic  
649 evolution of the Alborán sea, western Mediterranean. *Geochemistry, Geophysics, Geosystems* 8, n/a-n/a.  
650 <https://doi.org/10.1029/2007gc001639>
- 651 Borque, M.J., Alzola, A.S., Martín-Rojas, I., Alfaro, P., Molina, S., Cintas, S.R., Caderot, G.R., Lacy, C., Avilés,  
652 M., Olmo, A.H., Tortosa, F.J.G., Estévez, A., Gil, A.J., 2019. How Much Nubia-Eurasia Convergence Is  
653 Accommodated by the NE End of the Eastern Betic Shear Zone (SE Spain)? Constraints From GPS Velocities.  
654 *Tectonics* 38, 271–1839. <https://doi.org/10.1029/2018tc004970>
- 655 Braga, J.C., Martín, J.M., Quesada, C., 2003. Patterns and average rates of late Neogene–Recent uplift of the Betic  
656 Cordillera, SE Spain. *Geomorphology* 50, 3–26. [https://doi.org/10.1016/s0169-555x\(02\)00205-2](https://doi.org/10.1016/s0169-555x(02)00205-2)
- 657 Carbonell, R., Sallares, V., Pous, J., Dañobeitia, J.J., Queralt, P., Ledo, J.J., Dueñas, V.G., 1998. A multidisciplinary  
658 geophysical study in the Betic chain (southern Iberia Peninsula). *Tectonophysics* 288, 137–152.  
659 [https://doi.org/10.1016/s0040-1951\(97\)00289-8](https://doi.org/10.1016/s0040-1951(97)00289-8)
- 660 Clark, S.J.P., Dempster, T.J., 2009. The record of tectonic denudation and erosion in an emerging orogen: an apatite  
661 fission-track study of the Sierra Nevada, southern Spain. *Journal of the Geological Society* 166, 87–100.  
662 <https://doi.org/10.1144/0016-76492008-041>
- 663 Comas, M. C., J. J. Dañobeitia, J. Alvarez-Marín, and J. I. Soto (1995), Crustal reflections and structure in the  
664 Alboran Basin. Preliminary results of the ESCI-Alboran survey, *Rev. Soc. Geol. Esp.*, 8(4), 529 – 542.
- 665 Comas, M.C., García-Dueñas, V., Jurado, M.J., 1992. Neogene tectonic evolution of the Alboran Sea from MCS  
666 data. *Geo-mar Lett* 12, 157–164. <https://doi.org/10.1007/bf02084927>





- 667 Comas, M., and MARSIBAL 1-06 Scientific Party (2007). Preliminary results of Marsibal 1-06 cruise in the  
668 Alboran and western Algero-Balearic basins. *Geophys. Res. Abst.*, 9, 10871.
- 669 Conand, C., Mouthereau, F., Ganne, J., Lin, A.T., Lahfid, A., Daudet, M., Mesalles, L., Giletycz, S., Bonzani, M.,  
670 2020. Strain Partitioning and Exhumation in Oblique Taiwan Collision: Role of Rift Architecture and Plate  
671 Kinematics. *Tectonics* 39, e2019TC005798. <https://doi.org/10.1029/2019tc005798>
- 672 Couto, D.D., Gumiaux, C., Augier, R., Lebret, N., Folcher, N., Jouannic, G., Jolivet, L., Suc, J., Gorini, C., 2014.  
673 Tectonic inversion of an asymmetric graben: Insights from a combined field and gravity survey in the Sorbas  
674 basin. *Tectonics* 33, 1360–1385. <https://doi.org/10.1002/2013tc003458>
- 675 Crespo-Blanc, A., Comas, M., Balanyá, J.C., 2016. Clues for a Tortonian reconstruction of the Gibraltar Arc:  
676 Structural pattern, deformation diachronism and block rotations. *Tectonophysics* 683, 308–324.  
677 <https://doi.org/10.1016/j.tecto.2016.05.045>
- 678 d’Acremont, E., Lafosse, M., Rabaute, A., Teurquety, G., Couto, D.D., Ercilla, G., Juan, C., Lépinay, B.M.,  
679 Lafuerza, S., Galindo-Zaldivar, J., Estrada, F., Vazquez, J.T., Leroy, S., Poort, J., Ammar, A., Gorini, C., 2020.  
680 Polyphase Tectonic Evolution of Fore-Arc Basin Related to STEP Fault as Revealed by Seismic Reflection Data  
681 From the Alboran Sea (W-Mediterranean). *Tectonics* 39. <https://doi.org/10.1029/2019tc005885>
- 682 Dalziel, I.W.D., Lawver, L.A., Norton, I.O., Gahagan, L.M., 2013. The Scotia Arc: Genesis, Evolution, Global  
683 Significance. *Annu Rev Earth Pl Sc* 41, 767–793. <https://doi.org/10.1146/annurev-earth-050212-124155>
- 684 Daudet, M., Mouthereau, F., Bricchau, S., Crespo-Blanc, A., Gautheron, C., Angrand, P., 2020. Tectono-  
685 Stratigraphic and Thermal Evolution of the Western Betic Flysch: Implications for the Geodynamics of South  
686 Iberian Margin and Alboran Domain. *Tectonics* 39. <https://doi.org/10.1029/2020tc006093>
- 687 Dewey, J.F., 1988. Extensional collapse of orogens. *Tectonics* 7, 1123–1139.  
688 <https://doi.org/10.1029/tc007i006p01123>
- 689 Dewey, J.F., Helman, M.L., Knott, S.D., Turco, E., Hutton, D.H.W., 1989. Kinematics of the western  
690 Mediterranean. Geological Society, London, Special Publications 45, 265–283.  
691 <https://doi.org/10.1144/gsl.sp.1989.045.01.15>
- 692 Diaz, J., Gallart, J., Carbonell, R., 2016. Moho topography beneath the Iberian-Western Mediterranean region  
693 mapped from controlled-source and natural seismicity surveys. *Tectonophysics* 692, 74–85.  
694 <https://doi.org/10.1016/j.tecto.2016.08.023>
- 695 Duggen, S., Hoernle, K., Bogaard, P. van den, Harris, C., 2004. Magmatic evolution of the Alboran region: The role  
696 of subduction in forming the western Mediterranean and causing the Messinian Salinity Crisis. *Earth Planet Sc*  
697 *Lett* 218, 91–108. [https://doi.org/10.1016/s0012-821x\(03\)00632-0](https://doi.org/10.1016/s0012-821x(03)00632-0)
- 698 Duggen, S., Hoernle, K., Klügel, A., Geldmacher, J., Thirlwall, M., Hauff, F., Lowry, D., Oates, N., 2008.  
699 Geochemical zonation of the Miocene Alborán Basin volcanism (westernmost Mediterranean): geodynamic  
700 implications. *Contrib Mineral Petr* 156, 577. <https://doi.org/10.1007/s00410-008-0302-4>
- 701 Echeverria, A., Khazaradze, G., Asensio, E., Gárate, J., Dávila, J.M., Suriñach, E., 2013. Crustal deformation in  
702 eastern Betics from CuaTeNeo GPS network. *Tectonophysics* 608, 600–612.  
703 <https://doi.org/10.1016/j.tecto.2013.08.020>
- 704 Faccenna, C., Becker, T.W., Auer, L., Billi, A., Boschi, L., Brun, J.P., Capitanio, F.A., Funicello, F., Horváth, F.,  
705 Jolivet, L., Piromallo, C., Royden, L., Rossetti, F., Serpelloni, E., 2014. Mantle dynamics in the Mediterranean.  
706 *Rev Geophys* 52, 283–332. <https://doi.org/10.1002/2013rg000444>
- 707 Fortuin, A.R., Krijgsman, W., 2003. The Messinian of the Nijar Basin (SE Spain): sedimentation, depositional  
708 environments and paleogeographic evolution. *Sediment Geol* 160, 213–242. [https://doi.org/10.1016/s0037-0738\(02\)00377-9](https://doi.org/10.1016/s0037-0738(02)00377-9)
- 709 Fossen, H., Teyssier, C., Whitney, D.L., 2013. Transtensional folding. *Journal of structural geology* 56, 89–102.  
710 <https://doi.org/http://dx.doi.org/10.1016/j.jsg.2013.09.004>
- 711 Fossen, H., Tikoff, B., 1998. Extended models of transpression and transtension, and application to tectonic settings.  
712 Geological Society, London, Special Publications 135, 15–33. <https://doi.org/10.1144/gsl.sp.1998.135.01.02>
- 713 Frasca, G., Gueydan, F., Brun, J.-P., Monié, P., 2016. Deformation mechanisms in a continental rift up to mantle  
714 exhumation. Field evidence from the western Betics, Spain. *Mar Petrol Geol* 76, 310–328.  
715 <https://doi.org/10.1016/j.marpetgeo.2016.04.020>
- 716 Galindo-Zaldivar, J., Gonzalez-Lodeiro, F., Jabaloy, A., 2015. Progressive extensional shear structures in a  
717 detachment contact in the Western Sierra Nevada (Betic Cordilleras, Spain). *Geodin Acta* 3, 73–85.  
718 <https://doi.org/10.1080/09853111.1989.11105175>
- 719 Galindo-Zaldivar, J., Gil, A.J., Borque, M.J., González-Lodeiro, F., Jabaloy, A., Marin-Lechado, C., Ruano, P.,  
720 Galdeano, C.S. de, 2003. Active faulting in the internal zones of the central Betic Cordilleras (SE, Spain). *J*  
721 *Geodyn* 36, 239–250. [https://doi.org/10.1016/s0264-3707\(03\)00049-8](https://doi.org/10.1016/s0264-3707(03)00049-8)
- 722



- 723 Gallais, F., Graindorge, D., Gutscher, M.-A., Klaeschen, D., 2013. Propagation of a lithospheric tear fault (STEP)  
724 through the western boundary of the Calabrian accretionary wedge offshore eastern Sicily (Southern Italy).  
725 *Tectonophysics* 602, 141–152. <https://doi.org/10.1016/j.tecto.2012.12.026>
- 726 García-Dueñas, V., Banda, E., Torné, M., Córdoba, D., Group, E.-B.W., 1994. A deep seismic reflection survey  
727 across the Betic Chain (southern Spain): first results. *Tectonophysics* 232, 77–89. <https://doi.org/10.1016/0040->  
728 1951(94)90077-9
- 729 Giaconia, F., Booth-Rea, G., Martínez-Martínez, J.M., Azañón, J.M., Pérez-Romero, J., Villegas, I., 2013. Mountain  
730 front migration and drainage captures related to fault segment linkage and growth: The Polopos transpressive  
731 fault zone (southeastern Betics, SE Spain). *J Struct Geol* 46, 76–91. <https://doi.org/10.1016/j.jsg.2012.10.005>
- 732 Gomez-Pugnaire, M.T., Fernandez-Soler, J.M., 1987. High-pressure metamorphism in metabasites from the Betic  
733 Cordilleras (S.E. Spain) and its evolution during the Alpine orogeny. *Contrib Mineral Petr* 95, 231–244.  
734 <https://doi.org/10.1007/bf00381273>
- 735 Govers, R., Wortel, M.J.R., 2005. Lithosphere tearing at STEP faults: response to edges of subduction zones. *Earth*  
736 *Planet Sc Lett* 236, 505–523. <https://doi.org/10.1016/j.epsl.2005.03.022>
- 737 Haq, B., Gorini, C., Baur, J., Moneron, J., & Rubino, J.-L. (2020). Deep Mediterranean's Messinian evaporite giant:  
738 How much salt? *Global and Planetary Change*, 184, 103052.  
739 doi:<https://doi.org/10.1016/j.gloplacha.2019.103052>
- 740 Haughton, P.D.W., 2000. Evolving turbidite systems on a deforming basin floor, Tabernas, SE Spain.  
741 *Sedimentology* 47, 497–518. <https://doi.org/10.1046/j.1365-3091.2000.00293.x>
- 742 Haughton, P.D.W., 1994. Deposits of deflected and ponded turbidity currents, Sorbas Basin, Southeast Spain. *J*  
743 *Sediment Res* 64, 233–246. <https://doi.org/10.1306/d4267d6b-2b26-11d7-8648000102c1865d>
- 744 Heit, B., Mancilla, F. de L., Yuan, X., Morales, J., Stich, D., Martín, R., Molina-Aguilera, A., 2017. Tearing of the  
745 mantle lithosphere along the intermediate-depth seismicity zone beneath the Gibraltar Arc: The onset of  
746 lithospheric delamination. *Geophys Res Lett* 44, 4027–4035. <https://doi.org/10.1002/2017gl073358>
- 747 Hinsbergen, D.J.J., Vissers, R.L.M., Spakman, W., 2014. Origin and consequences of western Mediterranean  
748 subduction, rollback, and slab segmentation. *Tectonics* 33, 393–419. <https://doi.org/10.1002/2013tc003349>
- 749 Hodgson, D.M., Haughton, P.D.W., 2004. Impact of syndepositional faulting on gravity current behaviour and deep-  
750 water stratigraphy: Tabernas-Sorbas Basin, SE Spain. *Geological Soc Lond Special Publ* 222, 135–158.  
751 <https://doi.org/10.1144/gsl.sp.2004.222.01.08>
- 752 Janowski, M., Loget, N., Gautheron, C., Barbarand, J., BELLAHSEN, N., Driessche, J.V. den, Babault, J., Meyer,  
753 B., 2017. Neogene exhumation and relief evolution in the eastern Betics (SE Spain): Insights from the Sierra de  
754 Gador. *Terra Nova* 29, 91–97. <https://doi.org/10.1111/ter.12252>
- 755 Johnson, C., Harbury, N., Hurford, A.J., 1997. The role of extension in the Miocene denudation of the Nevado-  
756 Filábride Complex, Betic Cordillera (SE Spain). *Tectonics* 16, 189–204. <https://doi.org/10.1029/96tc03289>
- 757 Jolivet, L., Baudin, T., Calassou, S., Chevrot, S., Ford, M., Issautier, B., Lasseur, E., Masini, E., Manatschal, G.,  
758 Mouthereau, F., Thion, I., Vidal, O., 2021a. Geodynamic evolution of a wide plate boundary in the Western  
759 Mediterranean, near-field versus far-field interactions. *Bsgf - Earth Sci Bulletin* 192, 48.  
760 <https://doi.org/10.1051/bsgf/2021043>
- 761 Jolivet, L., Faccenna, C., 2000. Mediterranean extension and the Africa-Eurasia collision. *Tectonics* 19, 1095–1106.  
762 <https://doi.org/10.1029/2000tc900018>
- 763 Jolivet, L., Menant, A., Roche, V., Pourhiet, L.L., Maillard, A., Augier, R., Couto, D.D., Gorini, C., Thion, I.,  
764 Canva, A., 2021b. Transfer zones in Mediterranean back-arc regions and tear faults. *Bsgf - Earth Sci Bulletin*  
765 192, 11. <https://doi.org/10.1051/bsgf/2021006>
- 766 Jourdon, A., Kergaravat, C., Duclaux, G., Huguen, C., 2021. Looking beyond kinematics: 3D thermo-mechanical  
767 modelling reveals the dynamics of transform margins. *Solid Earth* 12, 1211–1232. [https://doi.org/10.5194/se-12-](https://doi.org/10.5194/se-12-1211-2021)  
768 1211-2021
- 769 Juan, C., Ercilla, G., Javier Hernández-Molina, F., Estrada, F., Alonso, B., Casas, D., . . . Ammar, A. (2016).  
770 Seismic evidence of current-controlled sedimentation in the Alboran Sea during the Pliocene and Quaternary:  
771 Palaeoceanographic implications. *Marine Geology*, 378, 292-311.  
772 doi:<https://doi.org/10.1016/j.margeo.2016.01.006>
- 773 Jurado, M.J., Comas, M.C., 1992. Well log interpretation and seismic character of the cenozoic sequence in the  
774 northern Alboran Sea. *Geo-Marine Letters* 12, 129–136.
- 775 Kleverlaan, K., 1989. Neogene history of the Tabernas basin (SE Spain) and its Tortonian submarine fan  
776 development. *Geologie en Mijnbouw* 421–432.
- 777 Kleverlaan, K., 1989. Three distinctive feeder-lobe systems within one time slice of the Tortonian Tabernas fan, SE  
778 Spain. *Sedimentology* 36, 25–45. <https://doi.org/10.1111/j.1365-3091.1989.tb00818.x>



- 779 Kleverlaan, K., 1987. Gordo megabed: a possible seismite in a tortonian submarine fan, tabernas basin, province  
780 almeria, southeast spain. *Sediment Geol* 51, 165–180. [https://doi.org/10.1016/0037-0738\(87\)90047-9](https://doi.org/10.1016/0037-0738(87)90047-9)
- 781 Koulali, A., Ouazar, D., Tahayt, A., King, R.W., Vernant, P., Reilinger, R.E., McClusky, S., Mourabit, T., Davila,  
782 J.M., Amraoui, N., 2011. New GPS constraints on active deformation along the Africa–Iberia plate boundary.  
783 *Earth Planet Sc Lett* 308, 211–217. <https://doi.org/10.1016/j.epsl.2011.05.048>
- 784 Larouzière, F.D.D., Bolze, J., Bordet, P., Hernandez, J., Montenat, C., d’Estevou, P.O., 1988. The Betic segment of  
785 the lithospheric Trans-Alboran shear zone during the Late Miocene. *Tectonophysics* 152, 41–52.  
786 [https://doi.org/10.1016/0040-1951\(88\)90028-5](https://doi.org/10.1016/0040-1951(88)90028-5)
- 787 Lonergan, L., White, N., 1997. Origin of the Betic-Rif mountain belt. *Tectonics* 16, 504–522.  
788 <https://doi.org/10.1029/96tc03937>
- 789 Mancilla, F. de L., Booth-Rea, G., Stich, D., Pérez-Peña, J.V., Morales, J., Azañón, J.M., Martín, R., Giaconia, F.,  
790 2015a. Slab rupture and delamination under the Betics and Rif constrained from receiver functions.  
791 *Tectonophysics*. <https://doi.org/10.1016/j.tecto.2015.06.028>
- 792 Mancilla, F. de L., Heit, B., Morales, J., Yuan, X., Stich, D., Molina-Aguilera, A., Azañón, J.M., Martín, R., 2018.  
793 A STEP fault in Central Betics, associated with lateral lithospheric tearing at the northern edge of the Gibraltar  
794 arc subduction system. *Earth Planet Sc Lett* 486, 32–40. <https://doi.org/10.1016/j.epsl.2018.01.008>
- 795 Mancilla, F. de L., Stich, D., Morales, J., Martín, R., Diaz, J., Pazos, A., Córdoba, D., Pulgar, J.A., Ibarra, P.,  
796 Harnafi, M., Gonzalez-Lodeiro, F., 2015b. Crustal thickness and images of the lithospheric discontinuities in the  
797 Gibraltar arc and surrounding areas. *Geophysical Journal International* 203, 1804–1820.  
798 <https://doi.org/10.1093/gji/ggv390>
- 799 Martín, J.M., Braga, J.C., Rivas, P., 1989. Coral successions in Upper Tortonian reefs in SE Spain. *Lethaia* 22, 271–  
800 286. <https://doi.org/10.1111/j.1502-3931.1989.tb01342.x>
- 801 Martín, JoséM., Braga, J.C., 1994. Messinian events in the Sorbas Basin in southeastern Spain and their implications  
802 in the recent history of the Mediterranean. *Sediment Geol* 90, 257–268. [https://doi.org/10.1016/0037-](https://doi.org/10.1016/0037-0738(94)90042-6)  
803 [0738\(94\)90042-6](https://doi.org/10.1016/0037-0738(94)90042-6)
- 804 Martínez-García, P., Comas, M., Lonergan, L., Watts, A.B., 2017. From Extension to Shortening: Tectonic  
805 Inversion Distributed in Time and Space in the Alboran Sea, Western Mediterranean. *Tectonics* 36, 2777–2805.  
806 <https://doi.org/10.1002/2017tc004489>
- 807 Martínez-García, P., Soto, J.I., Comas, M., 2011. Recent structures in the Alboran Ridge and Yusuf fault zones  
808 based on swath bathymetry and sub-bottom profiling: evidence of active tectonics. *Geo-mar Lett* 31, 19–36.  
809 <https://doi.org/10.1007/s00367-010-0212-0>
- 810 Martínez-Martínez, J.M., Azañón, J.M., 1997. Mode of extensional tectonics in the southeastern Betics (SE Spain):  
811 Implications for the tectonic evolution of the peri-Alborán orogenic system. *Tectonics* 16, 205–225.  
812 <https://doi.org/10.1029/97tc00157>
- 813 Martínez-Martínez, J.M., Booth-Rea, G., Azañón, J.M., Torcal, F., 2006. Active transfer fault zone linking a  
814 segmented extensional system (Betics, southern Spain): Insight into heterogeneous extension driven by edge  
815 delamination. *Tectonophysics* 422, 159–173. <https://doi.org/10.1016/j.tecto.2006.06.001>
- 816 Martínez-Martínez, J.M., Soto, J.I., Balanyá, J.C., 2002. Orthogonal folding of extensional detachments: Structure  
817 and origin of the Sierra Nevada elongated dome (Betics, SE Spain). *Tectonics* 21, 3-1-3–20.  
818 <https://doi.org/10.1029/2001tc001283>
- 819 Martínez-Martos, M., Galindo-Zaldívar, J., Martínez-Moreno, F.J., Calvo-Rayó, R., Galdeano, C.S. de, 2017.  
820 Superposition of tectonic structures leading elongated intramontane basin: the Alhabia basin (Internal Zones,  
821 Betic Cordillera). *Int J Earth Sci* 106, 2461–2471. <https://doi.org/10.1007/s00531-016-1442-9>
- 822 Meighan, H.E., Brink, U. ten, Pulliam, J., 2013. Slab tears and intermediate-depth seismicity: slab tears and  
823 intermediate seismicity. *Geophys Res Lett* 40, 4244–4248. <https://doi.org/10.1002/grl.50830>
- 824 Meijninger, B.M.L., Vissers, R.L.M., 2006. Miocene extensional basin development in the Betic Cordillera, SE  
825 Spain revealed through analysis of the Alhama de Murcia and Crevillente Faults: Miocene extensional basin  
826 development in the Betic Cordillera. *Basin Res* 18, 547–571. <https://doi.org/10.1111/j.1365-2117.2006.00308.x>
- 827 Montenat, C., D’Estevou, P.O., 1992. Geodynamics of the Eastern Betic late Neogene Basins. A Review. *Física de*  
828 *la Tierra* 57–75.
- 829 Mora, M., 1993. Tectonic and sedimentary analysis of the Huercal-Overa region, South East Spain, Betic Cordillera.  
830 University of Oxford, 300 pp.
- 831 Mouthereau, F., Angrand, P., Jourdon, A., Ternois, S., Fillon, C., Calassou, S., Chevrot, S., Ford, M., Jolivet, L.,  
832 Manatschal, G., Masini, E., Thion, I., Vidal, O., Baudin, T., 2021. Cenozoic mountain building and topographic  
833 evolution in Western Europe: impact of billions of years of lithosphere evolution and plate kinematics. *Bsgf -*  
834 *Earth Sci Bulletin* 192, 56. <https://doi.org/10.1051/bsgf/2021040>



- 835 Mouthereau, F., Filleaudeau, P., Vacherat, A., Pik, R., Lacombe, O., Fellin, M.G., Castellort, S., Christophoul, F.,  
836 Masini, E., 2014. Placing limits to shortening evolution in the Pyrenees: Role of margin architecture and  
837 implications for the Iberia/Europe convergence. *Tectonics* 33, 2283–2314. <https://doi.org/10.1002/2014tc003663>
- 838 Neuharth, D., Brune, S., Glerum, A., Morley, C.K., Yuan, X., Braun, J., 2021. Flexural strike-slip basins. *Geology*.  
839 <https://doi.org/10.1130/g49351.1>
- 840 Nocquet, J.-M., 2012. Present-day kinematics of the Mediterranean: A comprehensive overview of GPS results.  
841 *Tectonophysics* 579, 220–242. <https://doi.org/10.1016/j.tecto.2012.03.037>
- 842 Okay, A.I., Tüysüz, O., Kaya, Ş., 2004. From transpression to transtension: changes in morphology and structure  
843 around a bend on the North Anatolian Fault in the Marmara region. *Tectonophysics* 391, 259–282.  
844 <https://doi.org/10.1016/j.tecto.2004.07.016>
- 845 Palano, M., González, P.J., Fernández, J., 2015. The Diffuse Plate boundary of Nubia and Iberia in the Western  
846 Mediterranean: Crustal deformation evidence for viscous coupling and fragmented lithosphere. *Earth and*  
847 *Planetary Science Letters* 430, 439–447. <https://doi.org/10.1016/j.epsl.2015.08.040>
- 848 Palano, M., González, P.J., Fernández, J., 2013. Strain and stress fields along the Gibraltar Orogenic Arc:  
849 Constraints on active geodynamics. *Gondwana Res* 23, 1071–1088. <https://doi.org/10.1016/j.gr.2012.05.021>
- 850 Palomeras, I., Thurner, S., Levander, A., Liu, K., Villaseñor, A., Carbonell, R., Harnafi, M., 2014. Finite-frequency  
851 Rayleigh wave tomography of the western Mediterranean: Mapping its lithospheric structure. *Geochemistry,*  
852 *Geophysics, Geosystems* 15, 140–160. <https://doi.org/10.1002/2013gc004861>
- 853 Pedrera, A., Galindo-Zaldívar, J., Galdeano, C.S. de, López-Garrido, Á.C., 2007. Fold and fault interactions during  
854 the development of an elongated narrow basin: The Almanzora Neogene-Quaternary Corridor (SE Betic  
855 Cordillera, Spain): FOLD AND FAULT INTERACTIONS. *Tectonics* 26, n/a-n/a.  
856 <https://doi.org/10.1029/2007tc002138>
- 857 Pedrera, A., Galindo-Zaldívar, J., Ruiz-Constán, A., Duque, C., Marín-Lechado, C., Serrano, I., 2009. Recent large  
858 fold nucleation in the upper crust: Insight from gravity, magnetic, magnetotelluric and seismicity data (Sierra de  
859 Los Filabres–Sierra de Las Estancias, Internal Zones, Betic Cordillera). *Tectonophysics* 463, 145–160.  
860 <https://doi.org/10.1016/j.tecto.2008.09.037>
- 861 Pedrera, A., Galindo-Zaldívar, J., Tello, A., Marín-Lechado, C., 2010. Intramontane basin development related to  
862 contractional and extensional structure interaction at the termination of a major sinistral fault: The Huércal-  
863 Overa Basin (Eastern Betic Cordillera). *J Geodyn* 49, 271–286. <https://doi.org/10.1016/j.jog.2010.01.008>
- 864 Peña, L.G. de la, Grevemeyer, I., Kopp, H., Díaz, J., Gallart, J., Booth-Rea, G., Gràcia, E., Ranero, C.R., 2020a. The  
865 Lithospheric Structure of the Gibraltar Arc System From Wide-Angle Seismic Data. *J Geophys Res Solid Earth*  
866 125. <https://doi.org/10.1029/2020jb019854>
- 867 Peña, L.G. de la, Ranero, C.R., Gràcia, E., 2018. The Crustal Domains of the Alboran Basin (Western  
868 Mediterranean). *Tectonics* 37, 3352–3377. <https://doi.org/10.1029/2017tc004946>
- 869 Peña, L.G. de la, Ranero, C.R., Gràcia, E., Booth-Rea, G., 2020b. The evolution of the westernmost Mediterranean  
870 basins. *Earth-sci Rev* 103445. <https://doi.org/10.1016/j.earscirev.2020.103445>
- 871 Pickering, K.T., Hodgson, D.M., Platzman, E., Clark, J.D., Stephens, C., 2001. A New Type of Bedform Produced  
872 by Backfilling Processes in a Submarine Channel, Late Miocene, Tabernas-Sorbas Basin, SE Spain. *J Sediment*  
873 *Res* 71, 692–704. <https://doi.org/10.1306/2dc40960-0e47-11d7-8643000102c1865d>
- 874 Pindell, J.L., Kennan, L., 2009. Tectonic evolution of the Gulf of Mexico, Caribbean and northern South America in  
875 the mantle reference frame: an update. *Geological Soc Lond Special Publ* 328, 1–55.  
876 <https://doi.org/10.1144/sp328.1>
- 877 Platt, J.P., Behr, W.M., Johannesen, K., Williams, J.R., 2013. The Betic-Rif Arc and Its Orogenic Hinterland: A  
878 Review. *Annual Review of Earth and Planetary Sciences* 41, 313–357. <https://doi.org/10.1146/annurev-earth-050212-123951>
- 880 Platt, J.P., Kelley, S.P., Carter, A., Orozco, M., 2005. Timing of tectonic events in the Alpujarride Complex, Betic  
881 Cordillera, southern Spain. *J Geol Soc London* 162, 451–462. <https://doi.org/10.1144/0016-764903-039>
- 882 Platt, J.P., Vissers, R.L.M., 1989. Extensional collapse of thickened continental lithosphere: A working hypothesis  
883 for the Alboran Sea and Gibraltar arc. *Geology* 17, 540–543. [https://doi.org/10.1130/0091-7613\(1989\)017<0540:ecotcl>2.3.co;2](https://doi.org/10.1130/0091-7613(1989)017<0540:ecotcl>2.3.co;2)
- 884 Platt, J.P., Whitehouse, M.J., 1999. Early Miocene high-temperature metamorphism and rapid exhumation in the  
885 Betic Cordillera (Spain): evidence from U–Pb zircon ages. *Earth and Planetary Science Letters* 171, 591–605.
- 886 Platzman, E.S., 1992. Paleomagnetic rotations and the kinematics of the Gibraltar arc. *Geology* 20, 311–314.  
887 [https://doi.org/10.1130/0091-7613\(1992\)020<0311:pratko>2.3.co;2](https://doi.org/10.1130/0091-7613(1992)020<0311:pratko>2.3.co;2)
- 888





- 889 Poisson, A., Guezou, J.C., Ozturk, A., Inan, S., Temiz, H., Gürsöy, H., Kavak, K.S., ÖZDEN, S., 1996. Tectonic  
890 Setting and Evolution of the Sivas Basin, Central Anatolia, Turkey. *International Geology Review* 38, 838–853.  
891 <https://doi.org/10.1080/00206819709465366>
- 892 Poisson, A.M., Morel, J.L., Andrieux, J., Coulon, M., Wernli, R., Guemet, C., 1999. THE ORIGIN AND  
893 DEVELOPMENT OF NEOGENE BASINS IN THE SE BETIC CORDILLERA (SE SPAIN): A CASE STUDY  
894 OF THE TABERNAS-SORBAS AND HUERCAL OVERA BASINS. *J Petrol Geol* 22, 97–114.  
895 <https://doi.org/10.1111/j.1747-5457.1999.tb00461.x>
- 896 Pourhiet, L.L., Huet, B., May, D.A., Labrousse, L., Jolivet, L., 2012. Kinematic interpretation of the 3D shapes of  
897 metamorphic core complexes: 3D SHAPES OF MCCs. *Geochem Geophys Geosystems* 13.  
898 <https://doi.org/10.1029/2012gc004271>
- 899 Pownall, J.M., Hall, R., Watkinson, I.M., 2013. Extreme extension across Seram and Ambon, eastern Indonesia:  
900 evidence for Banda slab rollback. *Solid Earth* 4, 277–314. <https://doi.org/10.5194/se-4-277-2013>
- 901 Rat, J., Mouthereau, F., Bricchau, S., Crémades, A., Bernet, M., Balvay, M., Ganne, J., Lahfid, A., Gautheron, C.,  
902 2019. Tectonothermal Evolution of the Cameros Basin: Implications for Tectonics of North Iberia. *Tectonics* 38,  
903 440–469. <https://doi.org/10.1029/2018tc005294>
- 904 Rat, J., Mouthereau, F., Bricchau, S., Vacherat, A., Fillon, C., Gautheron, C., 2022. Timing and distribution of  
905 exhumation in the Ebro basin reveal a plate-scale 10 Ma geodynamic event. *Global Planet Change* 103973.  
906 <https://doi.org/10.1016/j.gloplacha.2022.103973>
- 907 Reicherter, K., Hübscher, C., 2006. Evidence for a seafloor rupture of the Carboneras Fault Zone (southern Spain):  
908 Relation to the 1522 Almería earthquake? *J Seismol* 11, 15–26. <https://doi.org/10.1007/s10950-006-9024-0>
- 909 Reinhardt, L.J., Dempster, T.J., Shroder, J.F., Persano, C., 2007. Tectonic denudation and topographic development  
910 in the Spanish Sierra Nevada. *Tectonics* 26, n/a-n/a. <https://doi.org/10.1029/2006tc001954>
- 911 Riding, R., Braga, J.C., Martín, J.M., Sánchez-Almazo, I.M., 1998. Mediterranean Messinian Salinity Crisis:  
912 constraints from a coeval marginal basin, Sorbas, southeastern Spain. *Mar Geol* 146, 1–20.  
913 [https://doi.org/10.1016/s0025-3227\(97\)00136-9](https://doi.org/10.1016/s0025-3227(97)00136-9)
- 914 Romagny, A., Jolivet, L., Menant, A., Bessière, E., Maillard, A., Canva, A., Gorini, C., Augier, R., 2020. Detailed  
915 tectonic reconstructions of the Western Mediterranean region for the last 35 Ma, insights on driving  
916 mechanisms. *Bsgf - Earth Sci Bulletin* 191, 37. <https://doi.org/10.1051/bsgf/2020040>
- 917 Rosenbaum, G., Lister, G.S., Duboz, C., 2002. Relative motions of Africa, Iberia and Europe during Alpine  
918 orogeny. *Tectonophysics* 359, 117–129. [https://doi.org/10.1016/s0040-1951\(02\)00442-0](https://doi.org/10.1016/s0040-1951(02)00442-0)
- 919 Sanz de Galdeano, C.S., Vera, J.A., 1992. Stratigraphic record and palaeogeographical context of the Neogene  
920 basins in the Betic Cordillera, Spain. *Basin Res* 4, 21–36. <https://doi.org/10.1111/j.1365-2117.1992.tb00040.x>
- 921 Sanz de Galdeano, C.S.D., Rodríguez-Fernández, J., López-Garrido, A.C., 1985. A strike-slip fault corridor within  
922 the Alpujarra Mountains (Betic Cordilleras, Spain). *Geol Rundsch* 74, 641–655.  
923 <https://doi.org/10.1007/bf01821218>
- 924 Sanz de Galdeano, C.S. de, Alfaro, P., 2004. Tectonic significance of the present relief of the Betic Cordillera.  
925 *Geomorphology* 63, 175–190. <https://doi.org/10.1016/j.geomorph.2004.04.002>
- 926 Scotney, P., Burgess, R., Rutter, E.H., 2000. 40Ar/39Ar age of the Cabo de Gata volcanic series and displacements  
927 on the Carboneras fault zone, SE Spain. *J Geol Soc London* 157, 1003–1008.  
928 <https://doi.org/10.1144/jgs.157.5.1003>
- 929 Sosson, M., Morrillon, A.-C., Bourgeois, J., Féraud, G., Poupeau, G., Saint-Marc, P., 1998. Late exhumation stages  
930 of the Alpujarride Complex (western Betic Cordilleras, Spain): new thermochronological and structural data on  
931 Los Reales and Ojen nappes. *Tectonophysics* 285, 253–273. [https://doi.org/10.1016/s0040-1951\(97\)00274-6](https://doi.org/10.1016/s0040-1951(97)00274-6)
- 932 Spakman, W., Wortel, R., 2004. The TRANSMED Atlas. The Mediterranean Region from Crust to Mantle 31–52.  
933 [https://doi.org/10.1007/978-3-642-18919-7\\_2](https://doi.org/10.1007/978-3-642-18919-7_2)
- 934 Stich, D., Serpelloni, E., Mancilla, F. de L., Morales, J., 2006. Kinematics of the Iberia–Maghreb plate contact from  
935 seismic moment tensors and GPS observations. *Tectonophysics* 426, 295–317.  
936 <https://doi.org/10.1016/j.tecto.2006.08.004>
- 937 Teyssier, C., Tikoff, B., 1998. Strike-slip partitioned transpression of the San Andreas fault system: a lithospheric-  
938 scale approach. *Geological Soc Lond Special Publ* 135, 143–158. <https://doi.org/10.1144/gsl.sp.1998.135.01.10>
- 939 Vacherat, A., Mouthereau, F., Pik, R., Bellahsen, N., Gautheron, C., Bernet, M., Daudet, M., Balansa, J., Tibari, B.,  
940 Jamme, R.P., Radal, J., 2016. Rift-to-collision transition recorded by tectonothermal evolution of the northern  
941 Pyrenees. *Tectonics* 35, 907–933. <https://doi.org/10.1002/2015tc004016>
- 942 Vázquez, M., Jabaloy, A., Barbero, L., Stuart, F.M., 2011. Deciphering tectonic- and erosion-driven exhumation of  
943 the Nevado-Filábride Complex (Betic Cordillera, Southern Spain) by low temperature thermochronology:



- 944 Deciphering tectonic- and erosion-driven exhumation. *Terra Nova* 23, 257–263. <https://doi.org/10.1111/j.1365->  
945 [3121.2011.01007.x](https://doi.org/10.1111/j.1365-3121.2011.01007.x)
- 946 Vergés, J., Fernández, M., 2012. Tethys–Atlantic interaction along the Iberia–Africa plate boundary: The Betic–Rif  
947 orogenic system. *Tectonophysics* 579, 144–172. <https://doi.org/10.1016/j.tecto.2012.08.032>
- 948 Vernant, P., Fadil, A., Mourabit, T., Ouazar, D., Koulali, A., Davila, J.M., Garate, J., McClusky, S., Reilinger, R.,  
949 2010. Geodetic constraints on active tectonics of the Western Mediterranean: Implications for the kinematics and  
950 dynamics of the Nubia-Eurasia plate boundary zone. *J Geodyn* 49, 123–129.  
951 <https://doi.org/10.1016/j.jog.2009.10.007>
- 952 Villasenor, A., Chevrot, S., Harnafi, M., Gallart, J., Pazos, A., Serrano, I., Córdoba, D., Pulgar, J.A., Ibarra, P.,  
953 2015. Subduction and volcanism in the Iberia–North Africa collision zone from tomographic images of the  
954 upper mantle. *Tectonophysics*. <https://doi.org/10.1016/j.tecto.2015.08.042>
- 955 Waldner, M., Bellahsen, N., Mouthereau, F., Bernet, M., Pik, R., Rosenberg, C.L., Balvay, M., 2021. Central  
956 Pyrenees Mountain Building: Constraints From New LT Thermochronological Data From the Axial Zone.  
957 *Tectonics* 40. <https://doi.org/10.1029/2020tc006614>
- 958 Weijermars, R., Roep, Th.B., Eeckhout, B.V. den, Postma, G., Kleverlaan, K., 1985. Uplift history of a Betic fold  
959 nappe inferred from Neogene-Quaternary sedimentation and tectonics (in the Sierra Alhamilla and Almeria,  
960 Sorbas and Tabernas Basins of the Betic Cordilleras, SE Spain). *Geologie en Mijnbouw* 397–411.
- 961 Zeck, H.P., Monié, P., Villa, I.M., Hansen, B.T., 1992. Very high rates of cooling and uplift in the Alpine belt of the  
962 Betic Cordilleras, southern Spain. *Geology* 20, 79. <https://doi.org/10.1130/0091->  
963 [7613\(1992\)020<0079:vhroca>2.3.co;2](https://doi.org/10.1130/0091-7613(1992)020<0079:vhroca>2.3.co;2)
- 964